MASTERARBEIT

Titel der Masterarbeit

Localization of $Ca_v1.3$ L-type calcium channels in the mouse retina

verfasst von

Christof Kugler, BSc

angestrebter akademischer Grad

Master of Science (MSc)

Wien, 2014

Studienkennzahl lt. Studienblatt:	A 066 834
Studienrichtung lt. Studienblatt:	Masterstudium Molekulare Biologie
Betreut von:	Univ. Prof. Mag. Dr. Alexandra Koschak

Acknowledgements

Table of Contents

1. Introduction

1.1. Ca²⁺ signaling

The bivalent calcium ion (Ca^{2+}) is an important intracellular messenger acting upon and regulating various cellular processes. The intracellular concentration of Ca^{2+}, $[Ca^{2+}]_i$, lies at about 10^{-7} M (mol l^{-1}), whereas its outside concentration, $[Ca^{2+}]_o$, (or in internal stores such as the endoplasmic reticulum) is fairly higher at ~ 10^{-3} M (*1*). To perform important signaling functions Ca^{2+} needs to be, on the one hand, a very fast messenger, e.g. at synaptic junctions, operating in a range of several microseconds. On the other hand, Ca^{2+} controls processes that need minute or hour long signaling, e.g. in gene transcription or cell proliferation events (*2*).

So-called on-reactions control Ca^{2+} entry into the cell. On the one hand, Ca^{2+} is released from internal stores, i.e. the endoplasmic reticulum or the sarcoplasmic reticulum in muscle cells, through various messenger molecules, e.g. inositol-1,4,5-trisphosphate (Ins(1,4,5)P₃), cyclic adenosine diphosphate ribose (cADPR) or nicotinic acid adenine dinucleotide phosphate (NAADP). On the other hand, Ca^{2+} enters the cell through channel proteins. These can be, e.g. voltage-operated channels (VOCs) – as outlined in section 1.2. (see below), receptor-operated channels (ROCs) – e.g. N-methyl-D-aspartate receptors (NMDARs), or second messenger operated channels (SMOCs) – e.g. cyclic nucleotide-gated channels (CNGCs) (*2*).

To fine tune Ca^{2+} signaling buffer proteins are present in the cytoplasm. These proteins bind Ca^{2+} during on-reactions and subsequently unload during off-reactions. Fast buffering proteins include Calbindin (CB) and Calretinin (CR), whereas Parvalbumin (PV) is characterized by slower binding kinetics toward Ca^{2+} (*2*)

To restore the physiological $[Ca^{2+}]_i$ four pumping mechanisms in the off-reaction are employed. The plasma membrane Ca^{2+}-ATPase (PMCA) and the sarco/endoplasmic reticulum Ca^{2+}-ATPase (SERCA) have low transport rates but high affinities to Ca^{2+}, meaning they are able to respond to modest changes in concentration. The Na^+/Ca^{2+} exchanger (NCX) and the mitochondrial uniporter employ faster transport rates and operate over a wide dynamic range (*2*).

In addition to these important reactions controlling intracellular Ca^{2+} concentrations, there is spatial and temporal organization of signaling events. Many Ca^{2+} signaling components form multi-structural complexes operating in very specific environments, e.g. NMDARs are linked to metabotropic glutamate receptors (mGluRs) and Ins(1,4,5)P₃Rs in neurons. Beyond the microsecond timescale of Ca^{2+} signaling, prolonged Ca^{2+} transients form so-called Ca^{2+} oscillations that have been shown to control a diverse range of cellular functions, e.g. neuronal cell migration. Longer Ca^{2+} transients trigger Ca^{2+} waves, sending a signal throughout the cell, e.g. in starburst amacrine cells of the retina (*2*).
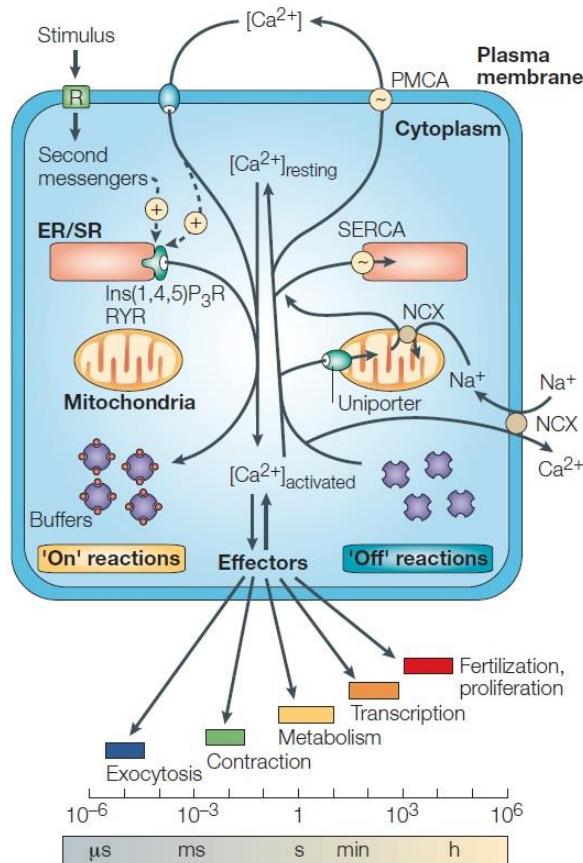
Figure 1 Calcium signaling pathways and homeostasis of its concentration gradient.

During on-reactions, calcium (Ca2+) enters the cell through specialized channel proteins or is released from second messenger-activated internal stores within the endoplasmic/sarcoplasmic reticulum (ER/SR). Ca2+ binds to its effectors, inducing a variety of cellular processes, or is taken up by buffering molecules. During off-reactions, Ca2+ is pumped into the ER/SR by SERCA, out of the cell by PMCA and NCX or into mitochondria by a uniporter (*2*).

1.2. Voltage-gated calcium channels

Voltage-gated calcium channels (VGCCs) belong to a protein superfamily of voltage-gated ion channels that all share a common pore-forming structural theme (*3*). In general, VGCCs mediate calcium ion influx into electrically excitable cells upon membrane depolarization, thereby regulating a diverse range of intracellular processes.

VGCCs can be divided into two distinct groups, based on their biophysical properties. The group of high-voltage activated (HVA) calcium channels contains the Ca_v1 (L-type) and Ca_v2 (N-, P/Q-, and R-type) channel families, whereas the low-voltage activated (LVA) group contains Ca_v3 channels (T-type).

The Ca_v1 family is comprised of four channels, i.e. $Ca_v1.1$, $Ca_v1.2$, $Ca_v1.3$, and $Ca_v1.4$. A common characteristic of Ca_v1 channels is the L-type current they elicit upon membrane depolarization. Such currents typically require a strong depolarization and are long-lasting. Channels of the Ca_v1 subfamily can be found in different cell types, e.g. muscle, endocrine and neuron, where they initiate contraction, secretion of hormones, regulation of gene expression, and release of neurotransmitters at specialized synapses in sensory cells, respectively. Channels of the Ca_v2 subfamily are characterized by N-, P/Q-, and R-type currents. These also require a strong depolarization to be activated. The three members ($Ca_v2.1$, $Ca_v2.2$, and $Ca_v2.3$) of this subfamily are primarily expressed in neurons, more specifically at synaptic terminals where they initiate neurotransmitter release and at cell bodies and dendrites where they mediate calcium entry into the cell (*4, 5*). Homologs of the Ca_v1 and Ca_v2 genes in the fruit fly *Drosophila melanogaster* have been shown to produce Ca^{2+} transients that trigger dendrite pruning in sensory neurons (*6*).

The Ca_v3 subfamily with its three members ($Ca_v3.1$, $Ca_v3.2$, and $Ca_v3.3$) is characterized by a T-type current. These currents require a weak depolarization in order to be activated and are transient, allowing Ca_v3 channels to shape action potentials and control patterns of repetitively firing cells. Consequently, they are found in neurons, cardiac, and smooth muscle myocytes where such properties are required (*4*).

1.3. L-type calcium channels

1.3.1. Structural organization of L-type calcium channels

L-type calcium channels (LTCCs) are multi-protein complexes composed of four to five different subunits that are expressed by multiple genes.
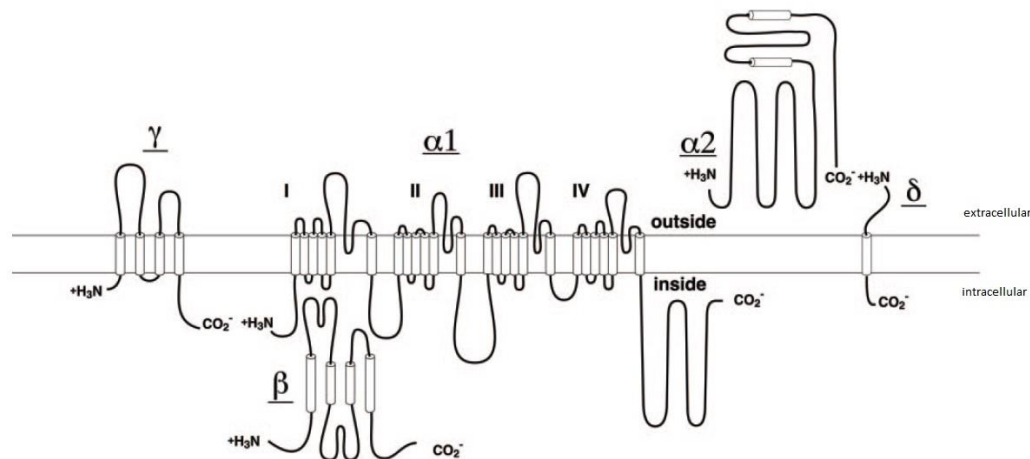
Figure 2 Subunit structure of L-type calcium channels.

Channels of the Ca$_v$1 family are composed of four to five different subunits. For details see text. Taken with modification from (4).

The α1 subunit is the largest subunit and incorporates the conduction pore, the voltage sensor and the gating apparatus. Furthermore, it harbors most known sites for channel regulation such as second messengers, drugs and toxins. It is organized in four homologous domains (domains I-IV) with six transmembrane segments (segments S1-S6) in each. Segment S4 serves as the voltage sensor, while segments S5 and S6 determine ion selectivity and conductance. The diversity of LTCCs in terms of electrophysiological and pharmacological properties is primarily based on different α1 subunits (4).

Ca$_v$1.1 and Ca$_v$1.4 channels are characterized by highly localized expression patterns. Ca$_v$1.1 is found in skeletal muscle transverse tubules where it mediates excitation-contraction coupling and Ca^{2+} homeostasis. Ca$_v$1.4, on the other hand, is mainly found in the retina where it initiates neurotransmitter release. Ca$_v$1.2 is characterized by a broad distribution across various tissues and, consequently, by the functions it fulfills. In cardiac and smooth muscle myocytes, Ca$_v$1.2 is responsible for excitation-contraction coupling and action potential propagation in sinoatrial and atrioventricular node. In endocrine cells, e.g. pancreatic β cells or cells of the pituitary, it mediates hormone release. And in neurons, Ca$_v$1.2 is involved in synaptic plasticity. Ca$_v$1.3 can also be characterized by a broad distribution pattern, e.g. sensory cells, endocrine cells, heart, vascular smooth muscle and neurons (4). For a more detailed introduction to Ca$_v$1.3, please see the next section (Section 1.3.2.).

Ca$_v$1.1	Skeletal muscle
Ca$_v$1.2	Cardiac, smooth muscle, neuronal
Ca$_v$1.3	Sinoatrial node, cochlear hair cells, neuronal
Ca$_v$1.4	Retina

Figure 3 Distribution patterns of L-type calcium channels.

Channels of the Ca$_v$1 family show a diverse range of localization across various tissues. Taken with modification from (7).

Functional LTCCs require so-called auxiliary subunits (besides the α1 subunit). The β subunit is located intracellularly and fulfills several functions, most importantly targeting of channel complexes to the plasma membrane (8). Furthermore, β subunits have been shown to modify electrophysiological and pharmacological channel properties (9). A single gene encodes for the α2δ pre-protein which is post-translationally cleaved into the α2 and δ subunits, respectively. The δ subunit spans the plasma membrane and is anchored to the extracellularly located α2 subunit via a disulfide bond. This α2δ subunit complex enhances channel expression and

influences/modifies channel properties (*7*). Recent work suggests that α2δ subunits are also involved in synaptogenesis and are GPI-anchored to the plasma membrane (*10*). A fifth auxiliary subunit, γ, has only been found in complexes with $Ca_v1.1$ and $Ca_v1.2$ channels, respectively, where it modulates biophysical properties (*4*).

1.3.2. Ca_v1.3 calcium channel

1.3.2.1. Ca_v1.3 calcium channel – gene and expression

The α1 subunit of $Ca_v1.3$ is encoded by the *CACNA1D* gene (*Homo sapiens*, NCBI gene ID: 776) and is comprised of 51 exons in humans. In the mouse (*Mus musculus*, NCBI gene ID: 12289) it is composed of 54 exons. There is, however, an extensive amount of alternative splicing which will be discussed in the next section (Section 1.3.2.2.).

1.3.2.2. Ca_v1.3 calcium channel – alternative splicing

Alternative splicing in $Ca_v1.3$ channels takes primarily place at hypervariable domains, including the intracellular C-terminus and the II-III intracellular linker sites (*11*).

Ca$_v$1.3 channels possess a so-called C-terminal modulatory domain (CTM) that reduces calmodulin (Cam)-dependent and Ca^{2+}-dependent inactivation (CDI) and promotes activation at more negative voltages. Two proposed α helices in the C-terminus, termed proximal C-terminal regulatory domain (PCRD) and distal C-terminal regulatory domain (DCRD), need to interact to elicit CTM (*12*). Recent publications have shown that alternative splicing can affect CTM. Alternative splicing of exon 41 can lead to deletion of the entire exon, causing a less pronounced CDI. Furthermore, it was shown that alternative splicing of exons 44 and 48 causes less robust CDI (*13*). Exon 42A, an alternatively spliced variant of exon 42, results in the truncation of 500 base pairs at the C-terminus (*14*), thereby lacking both PCRD and DCRD. In contrast, the gene product of alternative splicing in exon 43, employing exon 43S, lacks the DCRD but retains the PCRD (*15*).

1.3.2.3. Ca_v1.3 calcium channel – physiological role and tissue/cell type distribution

As stated in section 1.3.1., $Ca_v1.3$ channels are present in several different cell types and elicit various cellular processes. A knock-out mouse model shed light onto the importance of $Ca_v1.3$-mediated Ca^{2+}-currents for neurotransmitter release, namely glutamate, in cochlear inner hair

cells (IHCs). Due to the loss of neurotransmission in IHCs, $Ca_v1.3^{-/-}$ animals are deaf (*16*). Other studies have shown that $Ca_v1.3$ is present in endocrine cells, e.g. pancreatic β cells, adrenal chromaffin cells, pinealocytes and cells of the pituitary, where they regulate hormone secretion. Furthermore, $Ca_v1.3$ is expressed, at low density, in the heart (atrial muscle, sinoatrial and atrioventricular node) where it is important for the control of cardiac pacemaking and atrioventricular node conductance at rest. Also, $Ca_v1.3$ channels are present in neurons, primarily located at cell bodies and proximal dendrites (*4*). Recently it was shown that $Ca_v1.3$ channels are present in various regions of the mouse brain (*13*). Another study of $Ca_v1.3^{-/-}$ mice has revealed that $Ca_v1.3$ channels modulate the activity of neuronal networks in controlling mood behavior (*17*).

Recently, a 3 base pair insertion in the alternatively spliced exon 8B of human *CACNA1D* was found to result in the insertion of a glycine residue in the transmembrane helix IS6 of $Ca_v1.3$ channel proteins. Homozygous individuals carrying this mutation showed pronounced bradycardia and severe deafness. Electrophysiological experiments revealed several alterations in human mutant channels and the authors suggested, in conjunction with PCR data from mice, that exon 8B is predominantly present in human IHCs and SAN pacemaker cells. Consequently, they termed this disease sinoatrial node dysfunction and deafness (SANDD) (*18*).

Also, a recent report highlighted the pathophysiological effect of *CACNA1D* mutations in adrenal aldosterone producing adenomas (APAs), a (curable) form of hypertension. The authors identified several somatic mutations affecting functional domains, i.e. the channel activation gate, the voltage sensor and the S4-S5 linker. Electrophysiological studies pinpointed to gain of function phenotypes leading to enhanced aldosterone secretion, as suggested by the authors (*19*).

1.3.2.4. Ca$_v$1.3 calcium channel – functional properties

$Ca_v1.3$ channels activate at ~ -55 millivolt (mV) (*20*). This property is independent of tissue distribution or auxiliary subunits (*21*). Generally, LTCCs are sensitive to dihydropyridines. These can either act as agonists, i.e. enhancing calcium currents, e.g. BayK8644, or as antagonists, i.e. calcium channel blockers, e.g. nimodipine or isradipine. $Ca_v1.3$ is less sensitive to the calcium channel blocker isradipine (*21*) and shows fast activation kinetics (*20*), as compared to $Ca_v1.2$. These properties allow $Ca_v1.3$ to respond to physiological stimuli without activation of $Ca_v1.2$ (*20*), which is an important feature in cell types expressing both channels, e.g. neurons (*4*).

1.4. The retina

1.4.1. Structural organization and function

The vertebrate retina is a thin (approximate size ~ 200 µm), light-sensitive tissue of the central nervous system (CNS). It is located at the back of the eyeball in an inside-out-manner, meaning that photons, in order to reach photoreceptor cells, have to traverse the entire tissue before eliciting a response that will finally be processed by various different cell types within the retina. Integrated and processed signals will eventually leave the retina through its output neurons, i.e. ganglion cells, via the optic nerve to the brain.

The retina is a highly stratified tissue and contains two types of photoreceptor cells, i.e. rods and cones, which are supported by the above-lying retinal pigment epithelium (RPE). Furthermore, the retina contains four basic types of neuronal cells, i.e. horizontal cells, bipolar cells, amacrine cells and ganglion cells. In addition to that, one type of glial cell, i.e. Müller cells, is present (*22*).

The nuclei of all cells are concentrated in three nuclear layers, i.e. outer nuclear layer (ONL), inner nuclear layer (INL) and ganglion cell layer (GCL), which are separated from each other by two synaptic layers, i.e. outer plexiform layer (OPL) and inner plexiform layer (IPL) where signal processing and integration take place (*22*).
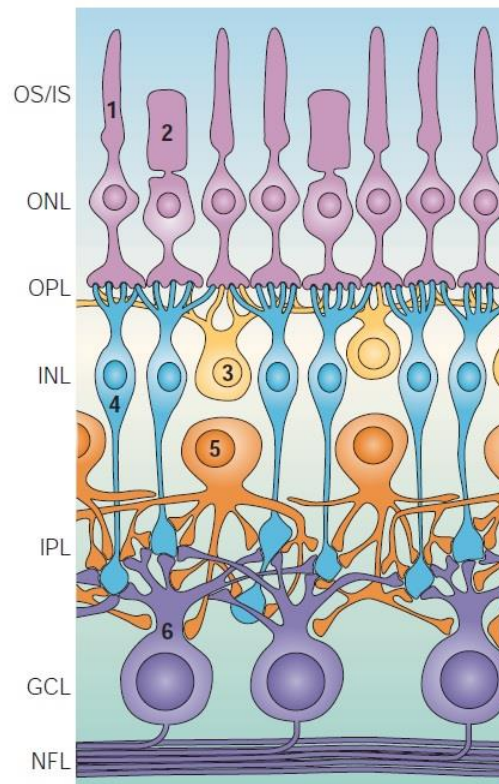
Figure 4 Organization of the vertebrate retina.

Rod (1) and cone (2) photoreceptor cells (PRs) have their nuclei in the first nuclear layer, the ONL. PRs form synapses in the OPL with horizontal (3) and bipolar (4) cells of the INL. Amacrine cells (5) have their cell bodies also in the INL. Amacrine and bipolar cells make synapses in the IPL with ganglion cells (6), the output neurons of the retina that relay the processed signal via the optic nerve fiber layer (NFL) to the brain. Taken from (*23*).

1.4.2. Cell types

1.4.2.1. The retinal pigment epithelium (RPE)

The RPE is a monolayer of pigmented cells, responsible for various functions in supporting and maintaining photoreceptor cells. The apical membrane of the RPE faces PR outer segments while the basolateral membrane faces capillaries of the choroid (*24*).

Pigmentation of the RPE guarantees absorption of scattered light, but more importantly, aids in the maintenance of visual function by concentrating light energy onto the retina. Due to the high blood supply from the choroid, photo-oxidation can be a problem, ultimately causing oxidative stress. To circumvent this problem, however, the RPE contains various pigments for filtering special wavelengths, as well as antioxidants and the ability to repair damaged DNA, lipids and proteins (*24*).

Another important function of the RPE is its involvement in the phototransduction cascade where the re-isomerization of the chromophore retinal takes place (for more details on the phototransduction cascade, see Section 1.4.2.2.). RPE cells serve in the maintenance of PR outer segments by continuous phagocytosis of shed segments. Furthermore, the RPE secretes various growth factors for structural maintenance and support to guarantee an optimal supply of nutrients (*24*). Interestingly, the RPE has been shown to contain $Ca_v1.3$ calcium channels which regulate secretion of angiogenic factors, i.e. vascular endothelial growth factor (VEGF) (*25*).

1.4.2.2. Photoreceptor cells (PRs)

In principle, there are two basic types of PRs – rods and cones. Rods contain the visual pigment rhodopsin and are responsible for vision under dark and dim conditions at night. Cones contain opsin molecules as visual pigments, and, depending on their wavelength sensitivity, can be classified into three groups (short wavelength (blue), middle wavelength (green) and long wavelength (red)). Cone PRs are responsible for color vision in bright light.

All four visual pigments are G-protein coupled receptors (GPCRs) and share a similar chemistry. In order to be photoactive, they are bound to a chromophore, i.e. retinal. The phototransduction cascade will be discussed for rod PRs.

In the dark, cyclic guanosine monophosphate (cGMP) is associated with cGMP-gated cation channels, which leads to an influx of cations, causing the cell to become depolarized. As a consequence, VGCCs (Ca$_v$1.4) are active, allowing an influx of Ca^{2+} which in turn leads to the release of the neurotransmitter glutamate. Upon absorption of photons, 11-*cis*-retinal in rod outer segments will isomerize to all-*trans*-retinal, ultimately changing the confirmation of rhodopsin. This conformational change results in the activation of the G-protein transducin, which activates cyclic GMP phosphodiesterase (PDE). PDE hydrolyzes cGMP, causing a decrease of cGMP levels in the cytosol. As a result, cGMP-gated cation channels will close, causing the cell to become hyperpolarized, which leads to termination of neurotransmitter release.

1.4.2.3. Horizontal cells

Mammalian retinae are thought to possess one to three types of horizontal cells (*22, 23, 26*). They extend processes into the OPL and primarily mediate lateral interactions (*22*). Furthermore, they provide feedback to PRs and possibly to dendrites of bipolar cells. Also, they measure the average level of illumination and process it to hold the signal that will be relayed to the inner retina in its operating range (*26*).

1.4.2.4. Bipolar cells

A recent study proposed that all major bipolar cell (BPC) types of the mouse retina appear to have been discovered. The number was put to 12, eleven cone bipolar cells and one rod bipolar cell (*27*).

BPCs can be classified into four distinct groups, i.e. ON, OFF, sustained, and transient. ON bipolar cells express the metabotropic glutamate receptor 6 (mGluR6), which, upon glutamate binding, causes closure of TRPM1 (transient receptor potential cation channel subfamily M member 1) cation channels. OFF BPCs express AMPA (α-amino-3-hydroxy-5-methyl-4-isoxazolepropionic acid) and kainate glutamate receptors, which are cation channels that open upon glutamate binding. Sustained and transient BPCs can be characterized by the expression of slowly or rapidly inactivating glutamate receptors (*26*).

BPC dendrites contact synapses of PRs, i.e. rod spherules and cone pedicles, in the OPL. BPC synapses form contacts with both amacrine and ganglion cells in the IPL. The IPL shows a very characteristic stratification, but in general can be separated into an OFF layer, which is on top of an ON layer (*23*).

1.4.2.5. Amacrine cells

Most amacrine cells appear to be axon-less (*22*) but share contacts to BPCs that drive them, form synapses with ganglion cells and have contacts to other, neighboring amacrine cells (*26*). Amacrine cells are difficult to classify and, due to a lack in identification methods, the exact number is not clear. Initial reports from rabbit, however, suggested that the number lies between 22 and 28 cells, respectively (*28*, *29*).

Generally, amacrine cells release inhibitory neurotransmitters, i.e. GABA (γ-Aminobutyric acid) and glycine, and perform 3 main functions. First, they create contextual effects for the responses of ganglion cells, e.g. object motion detection (which is required to distinguish object motion from self-induced motion of the observer). Second, they perform vertical integration between strata in the IPL, more specifically so-called cross-over inhibition. And third, they are highly specific for single tasks, e.g. A17 or starburst amacrine cells. The widely spreading A17 amacrine cell connects hundreds of synaptic boutons with the output sites of a rod bipolar cell (RBPC). There, it feeds back an inhibitory signal that improves the fidelity of information transmission by the RBPC (*26*, *30*).

1.4.2.6. Ganglion cells

Ganglion cells are the output neurons of the retina, relaying the processed signal via the optic nerve to the brain. The exact number of ganglion cells, however, is still unclear, but depending on interpretation and classification, lies around 20 (*22*, *26*).

The most striking property of ganglion cells is the receptive field, i.e. the illuminated part of the retina to which these cells respond. Ganglion cells showing contrast sensitivity in their receptive field can be divided into ON-center, OFF-surround, OFF-center and ON-surround, based on the spatial illumination, i.e. center or surround, and the answer it elicits, i.e. ON or OFF (*22*). Ganglion cells are, however, even more complex in terms of signal processing and integration. For a highly detailed overview of ganglion cell properties – which would go beyond the scope of this work – I recommend (*23*) & (*26*).

1.4.2.7. Müller cells

Müller cells are the primary glial cells of the retina. Their cell bodies are concentrated in the inner nuclear layer, however, they span the entire retina. Both plexiform layers receive branches from Müller cells, where neuronal processes and synapses are ensheathed (*31*).

Müller cells serve various important functions. One is neuroprotection against excitotoxic and oxidative damage. They express GLAST (Glutamate aspartate transporter), which helps in

the re-uptake of glutamate to protect against prolonged exposure to that neurotransmitter, and consequently, neurotoxicity. Furthermore, Müller cells possess glutathione, effectively protecting the retina against reactive oxygen species (*31*). Other functions include buffering of K^+ ions (taking up und redistributing excess K^+ ions), phagocytosis of neuronal debris and release of neuroactive substances (*32*).

1.4.3. Ca$_v$1.3 in the retina

There is a growing number of reports highlighting that *CACNA1D* mRNA and/or Ca$_v$1.3 protein is present throughout the mouse retina. However, as listed in Table 1, these studies provide a rather inconclusive picture as to where the gene product and/or the protein are exactly located.

Table 1 Detection of *CACNA1D* mRNA and/or Ca$_v$1.3 protein.

sc RT-PCR, single cell reverse transcription polymerase chain reaction; IF, immunofluorescence; ISH, in-situ hybridization; WB, Western Blot

Cell type(s)/layer(s)	Method(s)	Reference
AII amacrine cells (exclusively), ganglion cells (in conjunction with other VGCCs)	sc RT-PCR, electrophysiology	(*33*)
Cone PR terminals, OPL, ganglion cells	IF	(*34*)
ONL, INL, GCL	ISH	(*35*)
OPL, IPL	IF	(*36*)
All layers	IF	(*17*)
rod PRs, INL, GCL	RNA-ISH, immunoelectron microscopy	(*37*)
Unspecific staining pattern in wt and Cav1.3$^{-/-}$	WB, IF	(*38*)

Single cell reverse transcription polymerase chain reaction (sc RT-PCR) revealed that AII amacrine cells exclusively express *CACNA1D* mRNA, whereas retinal ganglion cells express six VGCCs, including *CACNA1D*. Furthermore, electrophysiological experiments in conjunction with pharmacological treatment resulted in the identification of L-type currents in AII amacrine cells (*33*). Incubating retina and brain tissue sections with two specific in-situ hybridization probes, on the other hand, revealed that *CACNA1D* mRNA is present in all three nuclear layers (*35*). Another study employing in-situ hybridization showed *CACNA1D* mRNA in the developing retina of the mouse embryo, and, in wild-type animals, gave a strong signal in the INL and GCL (*37*). However, recent transcriptome analyses of 22 transgenic mouse lines were not able to detect *CACNA1D* transcripts in murine retinae (*39*).

On the protein level, most studies applied immunofluorescence (IF) or Western Blotting (WB) experiments to detect Ca$_v$1.3 protein. Using an antibody directed against the C-terminus of Ca$_v$1.3 (*34*) were able to show that the protein is present in cone photoreceptor terminals, the OPL and in ganglion cells. In another study, retina cryo-sections were incubated with an anti-

Ca$_v$1.3 antibody, giving a signal in both OPL and IPL, as compared to control sections that were treated with peptide pre-incubated antibodies (*36*). In (*17*), retina cryo-sections of wild-type and Ca$_v$1.3$^{-/-}$ animals were probed with an anti-Ca$_v$1.3 antibody directed against the N-terminus. Staining was detectable in all retinal layers of the wild-type and completely absent in the knock-out. And vibratome-cut sections with subsequent immunoelectron microscopy revealed that Ca$_v$1.3 is present in rod photoreceptor outer and inner segments, as well as the synapse (*37*). In contrast to the IF experimental results from above, (*38*) were not able to show specific staining patterns in the mouse by employing at least three different anti-Ca$_v$1.3 antibodies.

Experimental data detecting *CACNA1D* mRNA and/or Ca$_v$1.3 protein in other species is also available. In-vitro cultures of human Müller cells in conjunction with RT-PCR hinted to the presence of *CACNA1D* mRNA (*40*). Developmental studies of African clawed frog (*Xenopus laevis*) using in situ hybridization revealed presence of *CACNA1D* mRNA in the retina, among several other tissues (*41*). In tree shrew (*Tupaia belangeri*) retina sections, Ca$_v$1.3 channels were detected in PR terminals in the OPL and along the outer border of the IPL by means of immunofluorescence (*42*). In tiger salamander (*Ambystoma tigrinum*) retina and brain extracts, Ca$_v$1.3 is detected via Western Blot. Furthermore, immunofluorescence of retina sections and isolated Müller cells revealed Ca$_v$1.3 staining in this cell type (*43*). Another study on salamander retina sections showed Ca$_v$1.3 localization in all three nuclear layers and in both synaptic layers. Double immunolabeling experiments revealed colocalization in Müller cells (*44*). Immunocytochemistry experiments on dissociated retinal cells from salamander suggest presence of Ca$_v$1.3 in amacrine and/or ganglion cells (*45*). And finally, in the rat (Sprague-Dawley) Ca$_v$1.3 immunoreactivity was present in PRs and the IPL. Most likely, also Müller cells were labeled (*46*). Immunofluorescence of rat (Wistar) retina sections showed localization in PR inner segments, the outer limiting membrane, the OPL and the IPL (*37*).

1.5. Mouse models

1.5.1. Ca$_v$1.3 DEME (HA-knock-in)

The generation of this mouse model can be read in detail in Anja Scharinger's dissertation (Univ. Prof. Jörg Striessnig, University of Innsbruck, Austria). The purpose of this mouse model was to study channel regulation by CTM. Furthermore, due to the presence of the easily detectable hemagglutinin (HA) epitope several detectability experiments can be performed (*47*).
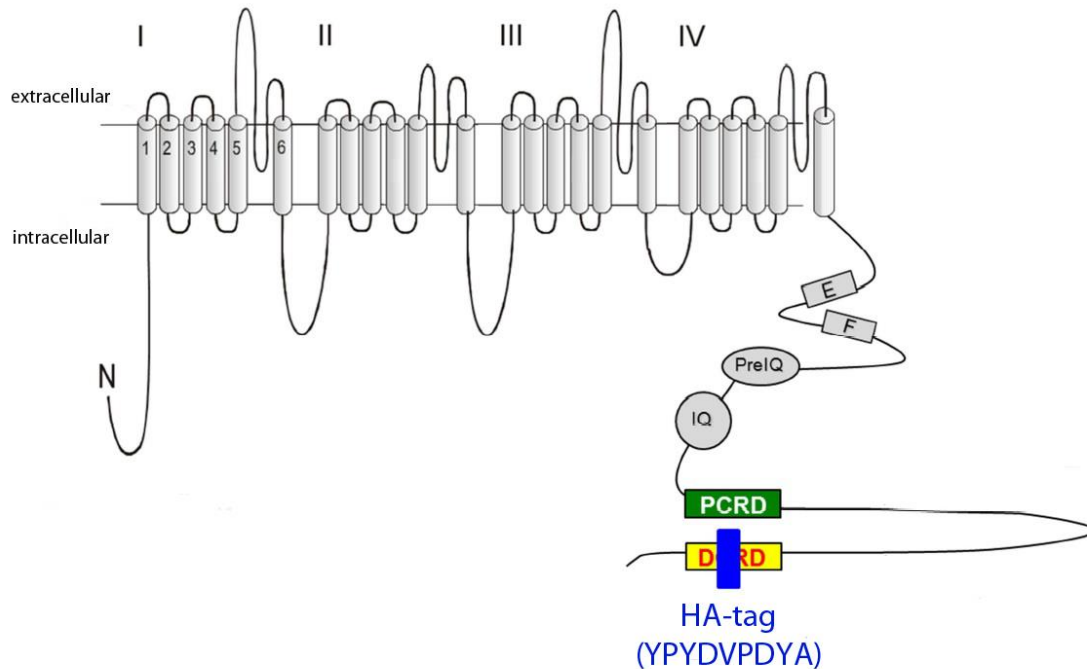
Figure 5 Insertion of HA-tag into DCRD of Ca$_v$1.3.

The native genomic region of Ca$_v$1.3 coding for the four amino acids DEME was replaced by a targeting construct via homologous recombination (not shown). The inserted construct codes for the nine amino acids comprising the HA-tag. All domains of Ca$_v$1.3 α1 subunit are shown, highlighting both PCRD (green box) and DCRD (yellow box) in which the HA-tag (blue box) was inserted. Taken with modification from (*47*).

Amino acid one-letter codes: A, alanine; D, aspartic acid; E, glutamic acid; M, methionine; P, proline; V, valine; Y, tyrosine

1.5.2. Ca$_v$1.3$^{-/-}$

The generation of this mouse model was done by J. Platzer et al. and can be read in their publication (*16*).

1.6. Aim of this study

Ca$_v$1.4, which is encoded by the *CACNA1F* gene, was recently identified to be the primary calcium channel in the retina. Mutations in this gene cause incomplete X-linked congenital stationary night blindness (*48*, *49*). Its main localization is the OPL, and colocalization experiments with synaptic markers revealed Ca$_v$1.4 presence at so-called synaptic ribbons (*34*, *50*, *51*). So far, however, Ca$_v$1.3 mRNA and protein have been shown to be also present in the mouse retina (Table 1). Furthermore, there are studies highlighting the presence of Ca$_v$1.3 in other species (Section 1.4.3.).

Table 1, in addition, provides a comprehensive overview of recent localization studies of Ca$_v$1.3 in the mouse retina. However, these approaches yielded no clear determination of *CACNA1D* expression and/or Ca$_v$1.3 localization. As a consequence we tried a different approach. By working with genetically modified mice, most importantly the Ca$_v$1.3-HA mouse, I set out to determine the exact localization of Ca$_v$1.3 in the retina by means of immunofluorescence with an anti-HA antibody. The highly immunogenic HA peptide is an easily recognizable target for modern antibodies, so I figured it would be a fairly straightforward process to determine the retinal distribution of epitope tagged Ca$_v$1.3. The second mouse, a Ca$_v$1.3 knock-out animal, was used to study the effectiveness of a Ca$_v$1.3-specific antibody. Furthermore, tissues lacking Ca$_v$1.3 channels were used as reliable negative controls in Western Blot and immunofluorescence experiments.

At last, I aimed to assess if, i) introduction of an HA-tag into the DCRD of Ca$_v$1.3, and ii) absence of the protein, confers any morphological change in the retina. I did so by performing immunofluorescence experiments on wild-type, Ca$_v$1.3-HA and Ca$_v$1.3$^{-/-}$ retina cryo-sections with several known markers.

2. Experimental Procedures

2.1. Amplification of mCaV1.3(1a)-8b-42-HA-pcDNA3 construct

2.1.1. Generation of competent cells

Escherichia coli (*E. coli*) DH5α cells were kindly provided by Prof. Dr. Jörg Striessnig's laboratory (University of Innsbruck) and were cultivated on solid LB and CG agar plates, respectively, or in liquid LB and CG medium, respectively.

Table 2 Protocol for the preparation of LB medium.

Liquid lysogeny broth (LB) medium (autoclaved)	Quantity	LB agar (autoclaved)	Quantity
Peptone	10 g	Peptone	10 g
Yeast extract	5 g	Yeast extract	5g
NaCl	10 g	NaCl	10 g
1 M NaOH to adjust pH to 7.3		Agar	15 g
H_2O to final 1 l		1 M NaOH to adjust pH to 7.3	
		H_2O to final 1 l	

Table 3 Protocol for the preparation of CG medium.

Liquid circle grow (CG) medium (autoclaved)	Quantity	CG agar	Quantity
CG	40 g	CG	40 g
1 M NaOH to adjust pH to 7.3		Agar	15 g
H_2O to final 1 l		1 M NaOH to adjust pH to 7.3	
		H_2O to final 1 l	

First, 33 µl of cell suspension were streaked on solid LB or CG agar plates, respectively, and incubated overnight at 37 °C. In total, I prepared 4 plates (3x DH5α & 1x negative control, i.e. MQ water instead of cells). The following day, growth of bacterial cultures was assessed. There were no colonies on the negative control plate.

Consequently, 1 clone from each plate was picked with a sterilized pipette tip and transferred into 40 ml liquid LB solution. One sterilized pipette tip without picking a colony was used as a negative control. All tubes were incubated under constant agitation at 37 °C and 220 rotations per minute (rpm) overnight (IKA, KS 4000 i control).

The next day, 4 ml of bacterial culture were transferred into 250 ml liquid SOB medium (Table 4). The optical density at 600 nm (OD_{600}) at this point was 0.009. To reach a sufficient initial OD_{600} of 0.05, I added another 20 ml of over-night culture. The OD_{600} reached a value of 0.05. This liquid culture was incubated at 37 °C and 220 rpm for ~ 3 hours. At that point, OD_{600}

reached a value of 0.45. All OD_{600} measurements were performed on a Hitachi U-2001 spectrophotometer.

Table 4 Composition of SOB medium.

Liquid SOB medium (autoclaved)	Quantity (g) / Concentration (mM)
Yeast extract	1.25 g
Tryptone	5 g
NaCl	10 mM
KCl	2.5 mM
$MgCl_2$ 6x H_2O	10 mM
$MgSO_4$ 7x H_2O	10 mM
H_2O to final 250 ml	

All subsequent steps were carried out with the bacteria on ice. The culture was split into 4x 50 ml centrifugation tubes and chilled for 10 minutes. Cells were centrifuged at 4,000 rpm for 10 minutes at 4 °C (centrifuge: Sorvall RC5C, rotor: Sorvall GSA). The supernatant was discarded and the pellets were resuspended in 20 ml TB solution (Table 5) each. After pooling, the solution was kept on ice for 10 minutes.

Table 5 Composition of TB medium.

Liquid TB medium (sterile filtered at 4 °C)	Concentration (mM)
PIPES	10
$CaCl_2$ 2x H_2O	15
KCl	250
MnCl2 4x H_2O	55
1 M KOH or 1 M HCl to adjust pH to 6.7	
H_2O to final 100 ml	

Cells in liquid TB medium were centrifuged again under the aforementioned conditions. After discarding the supernatant the pellet was resuspended in 20 ml liquid TB medium. Upon addition of 1.4 ml dimethyl sulfoxide (DMSO), competent cells were prepared as 50 µl aliquots and snap-frozen in liquid nitrogen before being stored at -80 °C.

2.1.2. Transformation and Plasmid Preparation

mCaV1.3(1a)-8b-42-HA-pcDNA3 plasmid DNA was also kindly provided by Prof. Dr. Jörg Striessnig's laboratory (*47*).

Four vials of competent DH5α cells were thawed on ice. Three vials received 100 ng of plasmid DNA while one received MQ water to serve as a negative control. Cells were carefully mixed by tapping against the vials and incubated for 30 minutes on ice.

The vials were put onto a thermomixer (Eppendorf, Thermomixer comfort) and incubated at 42 °C for exactly 90 seconds. After adding 1 ml of liquid CG medium to each vial cells were incubated at 37 °C and 300 rpm for 1 hour.

100 µl of the transformed cells were streaked on prewarmed (37 °C) CG agar plates supplemented with 50 µg ml^{-1} ampicillin. Plates were transferred to an incubator (Memmert 100-800) for overnight incubation at 37 °C.

The next day, bacterial growth was assessed. There were no colonies on the negative control and sporadic growth on the construct plates. Consequently, two colonies were picked with a sterilized pipette tip and put into 5 ml liquid CG medium supplemented with 50 µg ml^{-1} ampicillin. One sterilized pipette tip was used as a negative control. These pre-cultures were cultivated at 37 °C and 220 rpm for ~ 7 hours.

In the evening, two large overnight cultures were prepared. Two flasks containing 400 ml liquid CG medium supplemented with 50 µg ml^{-1} ampicillin each were inoculated with 1 ml of pre-culture. Both overnight cultures were cultivated at 37 °C and 220 rpm.

The next day, both cultures were chilled on ice and centrifuged at 5,500 rpm at 4 °C for 15 minutes (Sorvall RC5C, Sorvall GSA). The pellets were treated according to the Midi-Prep kit manual (Macherey-Nagel, NucleoBond Xtra Midi Plus EF). Finally, plasmid DNA was eluted in 300 µl TE-EF buffer provided with the Midi-Prep kit and quantified using a nanophotometer (Implen, P 300) with a lid factor of 50 (light path of 0.2 mm from the lid, which is put on top of the LabelGuard Microliter Cell). Plasmid DNA was subsequently stored at -20 °C.

2.1.3. DNA digestion and control PCR

All substances used for DNA digestion and gel electrophoresis were from ThermoScientific. One µg µl^{-1} plasmid DNA was mixed with 1 µl EcoRI, BglII or HindIII restriction enzyme respectively, 2 µl EcoRI buffer, buffer O or buffer R, respectively, and 16 µL DNase-free water. This solution was carefully mixed by tapping against the vial and spun down briefly on a bench centrifuge (Eppendorf, 5415R). The digestion set-up was incubated at the enzymes' optimal working temperatures (i.e. 37 °C for all enzymes) for 1-4 hours.

All 20 µl of digested construct DNA were mixed with 6x DNA loading dye and loaded onto a 1 % (w/v) agarose gel supplemented with 5 µl of Midori Green Advance (Nippon Genetics) to stain DNA bands. Six µl of marker DNA ladder (Thermo Scientific, GeneRuler 1kb DNA ladder), which ranges from 250 to 10,000 base pairs (bp), were also loaded. Electropheresis was started at a constant voltage of 100 V and let run for 55 minutes with BioRad's PowerPac Basic power

supply. Finally, DNA bands were visualized using the AlphaImager HP System (proteinsimple) with integrated software (Alpha View, version 3.4.0).

2.2. Experimental animals

2.2.1. Animal housing and processing

C57BL/6N wild-type, $Ca_v1.3$ DEME HA-knock-in and $Ca_v1.3$ knock-out mice were housed under aseptic conditions in a 12 h light/12 h dark cycle (light on from 7 am to 7 pm) according to institutional regulations. If not stated otherwise in each respective experimental procedures subsection all animals in experiments were age- and sex-matched.

Littermates (n=4-6) were caged and assigned a reference number - by clipping a mark to one ear - for controlling. Furthermore, a small piece of tail was cut off (i.e. mouse tail biopsy) for genotyping to check the respective genotype.

In general, mice were killed by cervical dislocation without anesthesia. Immediately afterwards, the spinal cord was cut through with crude surgical scissors and the eyes were dissected with precision surgical scissors on an agar plate (5 % w/v) filled with ice-cold 1x PBS. For more details on eye/retina processing and handling, please refer to the respective subsections 2.4.2. & 2.7.1. For details on whole brain isolation, please refer to subsections 2.4.3. & 2.7.2. At the end of each tissue isolation tail biopsies were taken to re-check the respective genotype.

2.2.2. Genotyping of experimental mice

Mouse tail biopsies were generally stored at -20 °C. DNA was isolated by adding 100 µl tail digestion buffer (Table 6) to each biopsy followed by overnight incubation (~ 12 h) at 57 °C and 300 rpm (Eppendorf, Thermomixer comfort).

Table 6 Composition of tail digestion buffer.

Tail digestion buffer	Concentration
Tris/HCl pH 8.8	10 mM
KCl	50 mM
Triton X-100	0.1 % (v/v)
Proteinase K	200 ng/ml
H_2O to final 100 ml	

To inactivate proteinase K samples were heated to 95 °C and incubated for 10 minutes followed by centrifugation for 6 minutes at 13,200 rpm (Eppendorf, 5415R). Isolated DNA was either used immediately after tail digestion or stored at -20 °C.

Genotyping was performed by PCR on a C1000 Thermal Cycler (Bio-Rad).

- Ca$_v$1.3 DEME HA-knock-in:

Table 7 Composition of PCR mix for genotyping of Ca$_v$1.3 DEME mice.

Genoytping of Ca$_v$1.3 DEME	1x [µl]
DNA	0.5
AS_geno_fwd_1 (10 pmol/µl)	1
AS_geno_rev_1 (10 pmol/µl)	1
AS_geno_rev_2 (10 pmol/µl)	1
DMSO	1
H$_2$O	20.5

This PCR mix was put into tubes containing Illustra puRETaq Ready to go PCR beads (GE Healthcare) which already contain Taq polymerase (~ 2.5 units), dNTPs (deoxyribonucleotides; 200 µM of dATP, dCTP, dGTP and dTTP each), stabilizers, BSA and reaction buffer .

Primer sequences:
- AS_geno_fwd_1: 5'-TCTGTGCTACGTCCCCAGTGCT-3'
- AS_geno_rev_1: 5'-GCAGCACTAGCGTAATCTGGAACAT-3'
- AS_geno_rev_2: 5'-CGTGCCCGTCTCTGGCTGGA-3'

Table 8 Expected lengths of PCR fragments in Ca$_v$1.3 DEME HA-knock-in genotypings.

Genotype	PCR fragment length [bp]
+/+ (wild-type)	535
+/- (heterozygous)	332 + 535 + 678
-/- (homozygous)	332 + 678

Table 9 PCR program for Ca$_v$1.3 DEME HA-knock-in genotypings.

step	Temperature [°C]	Time [min]
1	94	3
2	94	0.5
3	63	0.5
4	72	1.5
5	go to step 2	repeat 40x
6	72	15
7	12	indefinite

PCR products were subsequently loaded onto a 2 % (w/v) agarose gel supplemented with 5 µl of Midori Green Advance. Electrophoresis was performed with 90-100 V for 50-60 minutes. Bands were analyzed and visualized in Alpha View.

- Ca$_v$1.3 knock-out:

Table 10 Composition of PCR mix for genotyping of Ca$_v$1.3 knock-out mice.

Genoytping of Ca$_v$1.3 knock-out	1x [µl]
DNA	2
α1D AS (10pmol/µl)	1
α1D S (10pmol/µl)	1
α1D NEOS (10pmol/µl)	1
dNTPs (10mM/ml)	0.5
DMSO	2
10x buffer	4
Taq polymerase	0.2
H$_2$O	8.3

The PCR mix was put into standard PCR tubes (Peqlab).

Primer sequences:

α1D AS: 5'-TAC TTC CAT TCC ACT ATA CTA ATG CAG GCT-3'

α1D S: 5'-GCA AAC TAT GCA AGA GGC ACC AGA-3'

α1D NEOS: 5'-TTC CAT TTG TCA CGT CCT GCA CCA-3'

Table 11 Expected lengths of PCR fragments in Ca$_v$1.3 knock-out genotypings.

Genotype	PCR fragment length [bp]
+/+ (wild-type)	300
+/- (heterozygous)	300 + 450
-/- (homozygous)	450

Table 12 PCR program for Ca$_v$1.3 knock-out genotypings.

step	Temperature [°C]	Time [min]
1	92	2
2	54	0.33
3	72	0.5
4	92	0.42
5	54	0.33
6	72	0.42
7	go to step 2	repeat 34x

8	72	7
9	4	indefinite

PCR products were subsequently loaded onto a 1 % (w/v) agarose gel supplemented with 5 µl of Midori Green Advance. Electrophoresis was performed with 90-100 V for 50-60 minutes. Bands were analyzed and visualized in Alpha View.

2.3. Cell culture and transfection of mammalian cells

tsA-201 cells were cultivated at 37 °C and 10 % CO_2 in a humidified cell culture incubator (Thermo Scientific, Forma Series II Water-Jacketed CO_2 Incubator). Cells were cultured in Dulbecco's modified Eagle's medium (DMEM) high glucose [4.5 g l^{-1}] (PAA) supplemented with 10 % (v/v) fetal calf serum or fetal bovine serum (PAA) in 10 cm cell culture dishes.

For transfection, cells were grown to ~ 70 % confluence. Appropriate quantities of DNA (Table 13) were put in 1 ml serum-free DMEM and 12 µl of TurboFect Transfection Reagent (Thermo Scientific) were added. After incubation for 20 minutes at room temperature the total transfection mix was put into the culture dish in a drop-wise manner. Cells were put back to 37 °C and 10 % CO_2 for overnight incubation.

For protein expression and subsequent isolation (see 2.4.1.) 5 cell culture dishes for each set-up were prepared.

For immunocytochemistry (see 2.6.1.) 1 cell culture dish for each set-up was prepared. To avoid interferences concerning fluorescence microscopy eGFP was omitted.

Table 13 DNA quantities used for transfection experiments.

Plasmid DNA	Ca$_v$1.3-HA [µg]	Mock [µg]
α1	1	-
β3	1	1
α2δ-1	1	1
pUC	2	2
eGFP	0.025	0.025

2.4. Protein preparation & quantification

2.4.1. Protein preparation of transfected tsA-201 cells

Transfected tsA-201 cells were detached from a 10 cm cell culture dish with 3 ml 1x PBS. Since 5 plates per set-up were used the total amount of cells was collected in a 15 ml tube and

centrifuged for 5 minutes at 1,500 rpm and 4 °C (centrifuge: 5810R, rotor: F-34-6-38). After discarding the supernatant the cell pellet was resuspended in 1 ml lysis buffer (Table 14) and incubated on ice for 15 minutes.

The cell suspension was carefully pipetted up and down 50 times with a 200 µl pipette tip and pressed through a 0.4 mm thin canula (Braun) 6 times before being centrifuged for 20 minutes at 3,600 rpm and 4 °C on a bench centrifuge (Eppendorf, 5415R). The supernatant was transferred into 1.5 ml ultracentrifuge tubes (Beckmann) and centrifuged for 20 minutes at 30,900 rpm and 4 °C (ultracentrifuge: Beckman XL-90, rotor: 45 Ti).

The supernatant was discarded and the cell pellet was kept on ice for 30 minutes. Subsequently, 100 µl ice-cold lysis buffer were added and incubated for 60 minutes on ice. Prepared cell membranes were resuspended with a 0.4 mm thin canula (Braun) attached to a 1 ml syringe (Henry Schein). 25 µl of this membrane preparation were forwarded to protein quantification via the Lowry assay (Section 2.4.4.). The remaining 75 µl were split into 3x 25 µl aliquots which were snap-frozen in liquid nitrogen and stored at -80 °C.

Table 14 Composition of lysis buffer in cell and retina membrane preparation experiments.

Substance	Final concentration
Tris/HCl pH 7.4	10 mM
Aprotinin	154 nM
Trypsin inhibitor from chicken egg white	0.1 mg ml^{-1}
Pepstatin A, dissolved in 100 % EtOH	1 µM
Benzamidine hydrochloride hydrate	0.5 mM
Phenylmethanesulfonyl fluoride (PMSF), dissolved in 100 % EtOH	0.2 mM
Iodoacetamide	2 mM
Leupeptine trifluoroacetate salt	2.344 µM
H$_2$O to final 12.5 ml	

2.4.2. Protein preparation of dissected mouse retinae

C75BL/6N wild-type, Cav1.3 DEME HA-knock-in (both hetero- and homozygous) and Cav1.3 knock-out (homozygous) mice were killed through cervical dislocation. Eyes were dissected by cutting through the *Nervus opticus* and put immediately in ice-cold 1x PBS on an agar plate (5 % w/v). Under a stereo microscope (Nikon SMZ645; eyepiece: C-W10X/22) the cornea was cut open and the lens was removed. By applying equal pressure on two opposing sides of the eyecup the retina dissociated from the choroid and floated freely in 1x PBS. Retinae were collected in ice-cold 1.5 ml tubes and frozen in liquid nitrogen.

Four frozen retinae from 2 animals of each genotype were resuspended in 1 ml lysis buffer (Table 14) and incubated on ice for 15 minutes. All subsequent steps were carried out as described in the last two paragraphs in 2.4.1 (see above).

2.4.3. Protein preparation of whole mouse brains

Wild-type, homozygous HA-knock-in and homozygous knock-out mice were killed through cervical dislocation. The head was cut off completely and placed in a clean petri dish. After removing all fur and skin, the skull was slowly opened by inserting a thick pair of tweezers on the caudal side (where the head was cut off) by applying low pressure. Brains were carefully dissected out of the skull, put into 2 ml tubes and immediately frozen in liquid nitrogen.

One frozen brain of each genotype was thawed on ice, mixed with 5 ml homogenization buffer (Table 15) and homogenized with 15 strokes in a Dounce homogenizer (Braun) which was kept on ice. 1 ml of the homogenate was taken as a first fraction (=homogenate fraction), snap-frozen in liquid nitrogen and stored at -80 °C. Residual homogenate was centrifuged at 19,500 rpm (centrifuge: Sorvall, RC5C plus, rotor: SS-34) for 10 minutes at 4 °C. The supernatant represented the cytosolic fraction of which 1 ml was taken for storage at -80 °C. Residual supernatant was discarded and the pellet resuspended in 4 ml homogenization buffer. The centrifugation step was repeated with the same conditions. The supernatant was discarded and the pellet, representing the membrane fraction, was resuspended in 1 ml homogenization buffer and pressed through a 0.4 mm thin canula (Braun) 2 times. The membrane fraction was snap-frozen in liquid nitrogen and stored at -80 °C.

Table 15 Composition of lysis buffer in brain membrane preparation experiments.

Substance	Final concentration (mM)
$NaHCO_3$	20
PMSF, dissolved in 100 % EtOH	0.2
Iodoacetamide	2
Benzamidine hydrochloride hydrate	0.5

2.4.4. Protein quantification via the Lowry assay

The protein content in the respective samples was determined via the method of Lowry (*52*). For this, a BSA standard series, ranging from 10 to 200 µg ml^{-1} in 10 µg ml^{-1} increments, was prepared from a 2 mg ml^{-1} stock solution (ThermoScientific).

Protein samples were diluted 1:20, 1:40 and 1:80, respectively, in 3 separate vials in quantities of 100 µl per vial. BSA standards and three blind samples (only distilled water) were also adjusted to a volume of 100 µl per vial.

Each 100 µl dilution was mixed with 100 µl 0.1 % (w/v) SDS and 1 ml Folin I solution (Table 16). All samples were briefly vortexed (~ 5 seconds) and incubated at room temperature for 10 minutes. Subsequently, 100 µl of Folin II solution (Table 17) were added to each vial. After vortexing (~ 5 seconds) and brief centrifugation on a bench centrifuge (Eppendorf, 5415R) for ~

10 seconds, vials were covered with aluminum foil and incubated in the dark at room temperature for 30-40 minutes.

Measurements were performed on a Hitachi U-2001 spectrophotometer. Final protein concentration was calculated via:

$$c_{sample}\ [\mu g \times \mu l^{-1}] = A^{adjusted}_{750nm} \times factor_{\ Folin\ I} \times dilution_{\ sample}$$

Eq. 1 Equation used for the determination of sample protein concentration.

Absorbance of each sample was measured at 750 nm and multiplied by the factor of Folin I solution and the dilution factor of the sample. Final sample concentration was determined as the mean of 3 different dilution measurements.

Where - c is the concentration of the sample in $\mu g\ \mu l^{-1}$

   - $A^{adjusted}_{750nm}$ is the corrected absorbance of the sample (i.e. absorbance of blind samples have been subtracted from sample absorbance) at a wavelength (λ) of 750 nanometers (nm)

   - factor $_{Folin\ I}$ is the calculated factor of the Folin I solution (Equation 3)

   - dilution$_{sample}$ is the respective dilution (1:20, 1:40 or 1:80, respectively) of each sample

All of these calculations were performed in a Microsoft Office 2010 Excel spreadsheet.

The Folin I solution was usually stable for ~ 4-6 months at 4 °C. However, the factor (factor$_{Folin\ I}$) of the solution used for the quantification of protein samples was always determined anew each time a new measurement was carried out. Generally, the factor of Folin I was between 59.2 and 67.6.

Table 16 Composition of Folin I solution.

Folin I	
Solution 1	Solution 2
20 g Na_2CO_3 in 980 ml 0.1 M NaOH	0.2 g $C_4H_4KNaO_6$ * 4 H_2O (Potassium sodium tartrate tetrahydrate) in 20 ml H_2O
	add 0.1 g $CuSO_4$
Mix both solutions, protect from light and store at 4 °C for ~ 4-6 months!	

Table 17 Composition of Folin II solution.

Folin II
5 ml H_2O
5 ml Folin & Ciocalteau's phenol reagent
Mix and protect from light. Always prepare freshly!

To determine factor$_{Folin\ I}$ a BSA standard series ranging from 10 to 200 µg ml^{-1} and three blind samples (pure distilled water) were measured at λ=750 nm. Corrected absorbance of each standard (i.e. the mean blind sample absorbance has already been subtracted from each standard absorbance) was plotted against each standard and a linear regression was performed in a Microsoft Office 2010 Excel spreadsheet.

The resulting equation looked (in a generalized form) like this:

$$y = k \times x + d$$

Eq. 2 Generalized equation after linear regression.

For details see text.

factor$_{Folin\ I}$ was subsequently calculated as the inverse of the slope, i.e.:

$$factor_{Folin\ I} = 1 \div k$$

Eq. 3 Equation to determine the factor of Folin I solution.

After performing a linear regression of absorbance values in an Excel spreadsheet the resulting regression line was presented in a form as described in Eq. 2. The inverse of the slope of this regression was determined to represent the factor of Folin I solution.

2.5. Immunoblotting

2.5.1. Protein separation via SDS-PAGE

Sodium dodecyl sulfate polyacrylamide gel electrophoresis (SDS-PAGE) was used to separate proteins from membrane preparations under denaturing/reducing conditions. If not stated otherwise, all device components were from Bio-Rad's Mini PROTEAN Tetra Cell system.

In brief, all necessary components of the resolving gel (Table 20) were mixed thoroughly and poured between two glass plates resulting in a thickness of 1.5 mm and an approximate height of ~ 7.5 cm. The resolving gel solution (6 % polyacrylamide) was overlaid with 2-propanol to receive a sharp upper edge and prevent drying out. After ~ 45 minutes 2-propanol was discarded and the stacking gel solution (4 % polyacrylamide) was poured on top. In addition, a 10- or 15-slot comb was inserted. The resolving gel took ~ 30 minutes to fully polymerize.

One or two gels were run in one chamber at the same time. If only one gel was run, a Mini Cell Buffer Dam from Bio-Rad was used to prevent leakage of the assembly. The Tetra Cell running chamber was subsequently filled with 1x running buffer (Table 19) as indicated on the

outside of the device and the comb was removed. All slots were carefully cleared of gel remnants to avoid retaining of protein samples.

Thirty µg of protein were mixed with 6 µl 5x sample loading buffer (Table 18) and, where necessary, diluted with distilled water to reach a final volume of 30 µl. Samples were subsequently placed on a thermomixer (Eppendorf, Thermomixer comfort) and incubated at 57 °C for 15 minutes.

Denatured/reduced proteins and pre-stained molecular weight markers (Thermo Scientific, PageRuler Plus Prestained Protein Ladder & Spectra Multicolor Broad Range Protein Ladder) were loaded and the device was closed with a lid containing both electrodes connected to Bio-Rad's Power Pac 3,000 power source. Electrophoresis was started with a constant voltage of 100 V for 20 minutes. After this initial stacking, voltage was increased to 140 V and continued to run for ~ 50 minutes. The gel/s was/were then forwarded to tank Western Blotting.

Table 18 Composition of 5x and 1x SDS-PAGE loading buffer.

Substance	Concentration in 5x	Final conc. (1x)
Tris/HCl pH 6.8	312.5 mM	62.5 mM
SDS	20 % (w/v)	4 % (w/v)
Glycerol	50 % (v/v)	10 % (v/v)
β-Mercaptoethanol	10 % (v/v)	2 % (v/v)
Bromophenoleblue	0.05 % (w/v)	0.01 % (w/v)
H_2O to final 25 ml in 5x stock		

Table 19 1x running buffer used in SDS-PAGE experiments.

Substance	Final concentration
Tris base	25 mM
Glycine	192 mM
SDS	0.1 % (w/v)
H_2O to final 1 l	

Table 20 Composition of resolving and stacking gels.

Substance	Resolving gel (6 % polyacrylamide)	Stacking gel (4 % polyacrylamide)
H_2O	5.985 ml	3.35 ml
2 M Tris/HCl pH 8.8	1.875 ml	-
0.625 M Tris/HCl pH 6.8	-	1.0 ml
20 % (w/v) SDS	50 µl	25 µl
30 % / 0.8 % (w/v) Acrylamide/Bisacrylamide	2.0 ml	0.665 ml
10 % (w/v) Ammonium Persulfate (APS)	80 µl	40 µl
N,N,N',N'-Tetranethylethylenediamine (TEMED)	8 µl	4 µl

2.5.2. Protein transfer and detection via Western Blot

Separated proteins now within the SDS polyacrylamide gel were transferred onto a nitrocellulose membrane (Whatman Protran BA85; pore size: 0.45 μm) via means of 'wet' or tank blotting. If not stated otherwise, all device components were from Bio-Rad's Mini PROTEAN Tetra Cell system with Mini Trans-Blot Module.

First, a so-called blot sandwich was assembled: the black side of the gel holder cassette was covered with two foam pads which were soaked in ice-cold transfer buffer (Table 21). One appropriately cut (i.e. to match the size of the gel) blotting filter paper (Hartenstein GB33) was put on top and the gel was carefully placed onto it. The nitrocellulose membrane was carefully put onto the gel so that there was exact congruence. One blotting filter paper and two more foam pads completed the sandwich. Then, potential air-bubbles were carefully rolled out with a serological pipette. Finally, the gel holder cassette was closed with the white/transparent side on top. The electrode assembly was put into the chamber and filled with ice-cold transfer buffer. To provide further cooling, a cooling unit was inserted and the entire chamber was put into a box filled with ice. Protein transfer took place at a constant voltage of 100 V for 90 minutes (Bio-Rad's Power Pac 3,000).

Table 21 Composition of 1x transfer buffer used in Western Blotting experiments.

Substance	Final concentration
Tris base	25 mM
Glycine	192 mM
SDS	0.1 % (w/v)
Methanol (MeOH)	20 % (v/v)
H_2O to final 1 l	

After completion of the blotting procedure, the membrane was transferred into blocking buffer (Table 22) and incubated for 2 hours at room temperature. To check the efficiency of the transfer, protein staining of the gel was performed by immersing it into Coomassie staining solution (Table 23) for 2 hours at room temperature. The gel was subsequently de-stained overnight by putting it into distilled water.

Table 22 Composition of blocking buffer used in Western Blotting exeperiments.

Substance	Final concentration
Non-fat dry milk	5 % (w/v)
Gelatine from bovine skin type B	0.2 % (w/v)
Dissolve in wash buffer to final 150 ml	

Table 23 Composition of Coomassie staining solution.

Substance	Quantity
Coomassie Brilliant Blue R-250	2 g
Acetic Acid	75 ml
Ethanol (96 %)	500 ml
Water	425 ml

Then, the blocked membrane was cut into two pieces (cut was made around the 70 kiloDalton (kDa) marker band). The upper part of the membrane (ranging in size from ~ 70 kDa up to 260 kDa) was put into blocking solution containing an antibody directed against the HA epitope. The lower part (ranging in size from ~ 45 kDa to ~ 70 kDa) was put into blocking solution containing an anti-β-tubulin antibody. In general, incubation with primary antibodies took place overnight at 4 °C on a rotating platform (BOECO, MR-1 Mini Rocker-Shaker) and lasted ~ 18-20 hours.

Primary antibodies:
- rat-anti-HA High Affinity, Roche 11 867 423 001
- mouse anti-beta-tubulin, AbFrontier LF-MA20056

The next day, both membrane pieces were washed 5x 5 minutes with wash buffer (Table 24).

Table 24 Composition of wash buffer used in Western Blotting experiments.

Substance	Final concentration
Tris/HCl pH 7.4	20 mM
NaCl	150 mM
Triton X-100	0.5 % (v/v)
Tween 20	0.1 % (v/v)
H_2O to final 1 l	

Membranes were then incubated with blocking solutions containing appropriate secondary antibodies conjugated with horseradish peroxidase (HRP) to visualize protein bands on film or in an imaging device. Secondary antibodies were applied for 2 hours at room temperature.

Secondary antibodies:
- goat-anti-rat IgG peroxidase conjugated, Jackson Immuno Research 112-035-003
- ECL Mouse IgG, HRP-Linked Whole Ab (from sheep), GE Healthcare NA931

After a final wash step (5x 5 minutes) membranes were placed on a sheet of transparent plastic and carefully overlaid with ECL solution (Thermo Scientific, enhanced chemiluminescence) for 2-3 minutes. After removal of ECL solution the plastic sheet was put into the imaging device (AlphaInnotech, FluoChem HD2) and bands were visualized by the device's camera and respective software for 10 minutes (AlphaInnotech, AlphaEaseFC, version 6.0.2).

After successful imaging, incubated membranes were put into a closeable film cassette in a dark room and sheets of film (GE Healthcare, Amersham Hyperfilm ECL) were placed on top to capture emitted light. Exposure times typically ranged from 3, 5 to 10 minutes. Exposed films were subsequently developed in a Curix 60 tabletop processor (Agfa HealthCare).

2.5.3. Densitometric Analysis

Densitometric analysis was performed using the Fiji image processing package. As stated on its website (http://fiji.sc/Fiji; accessed on March 20th, 2014) Fiji is a distribution of ImageJ (US NIH, United States National Institutes of Health), Java (Oracle Corp.) and several other plugins to assist research in life sciences. The version of ImageJ used in the analysis was 1.48r.
In brief, 16-bit tagged image file format (tiff) images were opened in ImageJ. Each lane on the blot image was marked with a rectangular selection tool provided with the program and the overall profile plot of each lane was visualized (this profile plot, in general, represents the density of all the content in each rectangularly selected lane in form of peaks with certain heights and widths).

Due to the low background levels on my blots I only observed one or two clearly distinguishable peaks on each rectangular selection. To evaluate these specific bands each peak was cut off from the baseline which can be interpreted as minor background signal. This was done by closing the peak from the horizontal background level with a straight line. Next, the area under each peak was calculated by ImageJ with the 'wand' tool. Area values (i.e. densities) of each sample were copied into a Microsoft Office 2010 Excel spreadsheet for further analysis.

First, loading control (i.e. β-tubulin) densities of each sample (wild-type, heterozygous & homozygous HA-knock-in) were put in relation to the wild-type level. The same was done for each HA signal band. Adjusted relative densities were obtained by dividing the relative density of each HA sample band by the relative density of the corresponding β-tubulin band. These normalized data were copied into a Prism file (GraphPad Software, Inc.; version 5.04) where statistical analysis and graph representation were performed.

2.5.4. Statistical Analysis

Statistical analyses of relative densities were performed in GraphPad Prism.

Retina membrane preparations were analyzed by a one-way analysis of variance (ANOVA). To compare all pairs of columns in the data sheet Tukey's multiple comparison test was applied in conjunction. The level of significance (α) was set to 0.01 (1 %).

Relative densities of brain membrane preparations were assessed by a paired, two-tailed t-test with a significance level of 0.01.

2.6. Immunocytochemistry

2.6.1. Transfection of mammalian cells

For transfection details please refer to section 2.3. After overnight incubation transfected cells were harvested in 1x PBS and centrifuged at 680 rpm for 5 minutes (Eppendorf, 5810). The cell pellet was resuspended in cell culture medium and cells were subsequently re-plated in a 6-well plate containing medium and poly-D-lysine (PDL)-coated coverslips (14 mm diameter). Cells were subsequently allowed to settle for another 24 hours at 37 °C and 10 % CO_2.

2.6.2. Fixation of transfected cells

All steps were carried out in a laminar flow hood at room temperature. Cell culture medium was removed by vacuum suction and cells were gently rinsed with 1x PBS. Each well was then filled with 3 ml of 2 % (w/v) paraformaldehyde (PFA) solution (PFA in 1x PBS) and cells were fixed for 20 minutes. After fixation, cells were washed with 1x PBS for 30 minutes in 5 changes. Cells were stained immediately post-fixation.

2.6.3. Staining of fixed cells

Coverslips were taken out of the 6-well plate and put onto a sheet of parafilm in a sealable container supplemented with H_2O-soaked paper tissues to provide a moist environment. All steps were performed at room temperature. Each coverslip was overlaid with 100 μl blocking/permeabilization buffer (Table 25) for 30 minutes.

Table 25 Composition of blocking buffer used in immunocytochemistry.

Substance	Final concentration
BSA	0.2 % (w/v)
Triton X-100	0.2 % (v/v)
Normal goat serum (NGS)	5 % (v/v)
Dissolve in 1x PBS to final 10 ml	

Blocking/permeabilization buffer was removed by suction with a bench pump (VACUSIP, INTEGRA) and the primary antibody (rat-anti-HA High Affinity, Roche 11 867 423 001) - diluted 1:1,000 in wash buffer (Table 26) – was applied for 4 hours.

Table 26 Composition of wash buffer in immunocytochemistry.

Substance	Final concentration
BSA	0.2 % (w/v)
Triton X-100	0.2 % (v/v)
Dissolve in 1x PBS to final 10 ml	

Upon removal of the primary antibody solution, coverslips were washed 30 minutes with wash buffer (5-6 changes of wash buffer) and the secondary antibody (Alexa Fluor® 594 Goat Anti-Rat IgG (H+L), Invitrogen A11007) – diluted 1:4,000 in wash buffer – was applied for a 1 hour incubation in the dark. From now on, every step was performed with the lights turned off. Coverslips were subsequently washed again for 30 minutes before nuclear staining with 10 ng ml^{-1} DAPI (4',6-diamidino-2-phenylindole) for 3 minutes. Finally, coverslips were washed again with wash buffer for 15 minutes (3x 5 minutes each) before being placed on an object slide supplemented with 1 drop of AquaPoly/Mount-Gel (Polysciences, Inc.) for each coverslip. After air-drying for 20-30 minutes, coverslips were sealed with commercially-available nail-polish and slides were stored protected from light at 4 °C.

2.6.4. Image acquisition and analysis

All fluorescence microscopy images shown in this work were taken at VetImaging, a core facility at the University of Veterinary Medicine, Vienna, Austria. The microscope was an upright, widefield microscope from Zeiss microscopy (AxioImager Z2).

Exposure times for all respective fluorescence excitation channels were set to equal values to guarantee comparability among samples. The camera was an AxioCam MRc5. If not stated otherwise, a 63x objective (63x/1.4 Plan-Apochromat, Oil, DIC) was used. Raw Carl Zeiss images (.czi) were transformed into JPEG files by the Carl Zeiss ZEN 2012 image software (blue edition). Subsequent picture analysis and creation of figures for this work were carried out in Adobe Photoshop CS5 Extended (version 12.0.4) from Adobe Systems, Inc.

2.7. Immunohistochemistry

In my diploma thesis I developed the method of immunohistochemistry to localize the HA-tagged $Ca_v1.3$ channel. As a consequence, several parameters in the following protocols were variable and changed according to developmental outcome.

2.7.1. Tissue preparation, fixation and embedding of eyecups

C75BL/6N wild-type, $Ca_v1.3$ DEME homozygous HA-knock-in and $Ca_v1.3$ homozygous knock-out mice were killed through cervical dislocation. Eyes were dissected by cutting through the *Nervus opticus* and put into a petri dish containing fixative solution. Each eyeball was placed on a fixative-soaked tissue paper and was handled separately.

First, the cornea was slightly cut with a sharp razorblade to allow infiltration of the eyeball with fixative. After 10 minutes of incubation the cornea was removed and the lens was dissected. For this, the zonule fibers, which connect the lens to the ciliary body of the eye, had to be cut through thoroughly. Once the lens was removed the eyecup was put back into fixative for 10 minutes. This was the standard protocol (indicated by red asterisk in Table 27).

Then, the eyecup was washed 4x with 1x PBS before being put into a solution of 30 % (w/v) sucrose in 1x PBS to cryo-protect the tissue. Eyecups were kept in this solution for 24 hours at room temperature on a rotating platform. The next day, eyecups were transferred into a 1:2 mix of 30 % sucrose solution and optimal cutting temperature (OCT) compound (Sakura, Tissue-Tek OCT Compound) for another 24 hours of incubation at room temperature.

Finally, eyecups were oriented in a dorsal-ventral manner on a petri dish under a stereo microscope. Orientation was solely based on visual inspection of blood vessels projecting to the optic nerve. However, orientation can be confirmed post-staining with adequate antibodies. Eyecups were subsequently placed in a cylinder containing a 1:2 mix of 30 % sucrose and OCT compound before immersion in liquid nitrogen-cooled isopentane. Complete freezing of these cylinders took about 20-25 seconds. Frozen cylinders were stored at -20 °C.

Generalized protocol of eyecup preparation, fixation and embedding:

Killing of animal ⟶ cut cornea $\xrightarrow{\text{incubate}}$ take out lens $\xrightarrow{\text{inc.}}$ wash in 1x PBS ⟶ put into 30 % sucrose solution $\xrightarrow{\text{24 h}}$ put into 30 % sucrose/OCT mix (1:2) $\xrightarrow{\text{24 h}}$ embed by immersing in liquid nitrogen-cooled isopentane

The type of fixative and fixation time was changed according to experimental outcome and reasoning. Table 27 gives an overview of all fixatives used and their respective incubation time with the tissue. For methanol and acetone fixation, both solutions were cooled to -20 °C and

eyecups were fixed after cryo-sectioning (i.e. eyes were not prepared (cornea cut & lens out) but remained completely intact and were frozen immediately after dissection).

Table 27 Summary of all fixatives used, including their respective incubation time with the tissue.

Condition denoted by red asterisk indicates standard practice.

Fixative	Fixation time (min)
2 % (w/v) Paraformaldehyde (PFA)	10
2 % PFA	20 (2x 10) *
4 % PFA	15
4 % PFA	120
Zamboni's	8
Methanol	15
Acetone	15

2.7.2. Tissue preparation, fixation and embedding of whole brains

Whole brains of C75BL/6N wild-type, homozygous $Ca_v1.3$-HA-knock-in and homozygous $Ca_v1.3$ knock-out mice were dissected by opening the skull with crude surgical scissors and removed with tweezers. Brains were briefly washed in ice-cold 1x PBS (5 minutes) before being immersion-fixed in 2 % PFA for 24 hours at 4 °C. After washing in ice-cold 1x PBS brains were cryo-protected in 30 % sucrose for 2 days at 4 °C. Finally, whole brains were incubated in a 1:2 mix of 30 % sucrose/OCT compound for 30 minutes, oriented in a way so that coronal sections could be cut and embedded in cylinders containing 30 % sucrose/OCT (1:2) by immersion into liquid nitrogen-cooled isopentane. Cylinders were stored at -20 °C.

2.7.3. Cryo-sectioning

Eyecups and whole brains were cryo-sectioned in a Leica cryo-stat (CM1950) to a thickness of 16 µm, and 20 µm, respectively.

Briefly, frozen cylinders were placed onto a specimen disc which was mounted onto an orientable specimen head. After checking the right angle for sectioning frozen cylinders were first trimmed until the optic nerve or frontal cortex was clearly visible by checking under a light microscope. Subsequently, 16 µm and 20 µm thick cryo-sections were cut with low-profile microtome blades (ThermoScientific, MX35 Premier+) and taken onto positively-charged glass

slides (ThermoScientific, SuperFrost Plus). Cryo-sections were finally air-dried at room temperature for ~ 1 hour before being stored at -20 °C.

2.7.4. Staining of retina cryo-sections

Slides containing sections from the same eccentricity, i.e. same distance from the optic nerve, were air-dried at room temperature for 1-2 hours before being encircled with commercially-available nail-polish to create a reservoir for blocking and antibody solutions. After another 15 minutes of drying, sections were either 1) forwarded to antigen retrieval or 2) immediately washed with wash buffer (Table 29) 3x 10 minutes.

1) Antigen retrieval is a method commonly used when it is suspected that the target epitope is masked, e.g. by over-fixation of the specimen. There are several protocols available of which I tried 3:

Table 28 Antigen retrieval buffers #1 (Tris/EDTA, top) and #2 (Citrate, bottom).

Substance	Final conc.
Tris base	10 mM
EDTA	1 mM
Dissolve in H_2O to final 500 ml, pH ~ 9.0	
Tween 20	0.05 % (v/v)

Substance	Final conc.
Citric acid (anhydrous)	10 mM
Dissolve in H_2O to final 500 ml	
1 M NaOH to adjust pH to 6.0	
Tween 20	0.05 % (v/v)

Buffers were heated to ~ 95 °C in a water bath. Glass slides containing cryo-sections were put into these buffers and incubated for 20 minutes. After that, washing steps with wash buffer and the remaining procedure were carried out.

The third solution I tried was a 1 % (w/v) SDS solution in 1x PBS. Sections were first washed with 1x PBS 3x 5 minutes before being immersed in SDS solution for 5 minutes. After a single wash in 1x PBS, sections were washed with wash buffer and treated according to protocol.

2) If antigen retrieval was not performed, sections were immediately washed 3x 10 minutes.

Table 29 Composition of wash buffer used in retina immunohistochemistry.

Substance	Final concentration
Triton X-100	0.1 % (v/v)
NaN$_3$	0.05 % (w/v)
Dissolve in 1x PBS to final 1 l	

Sections were subsequently incubated with blocking buffer (Table 30) to prevent unspecific binding of antibodies. To develop the best blocking result several different buffers have been tested.

Table 30 Summary of all blocking reagents and incubation times used in blocking buffers for retina immunohistochemistry.

Condition denoted by red asterisk indicates standard practice.

Substance, in wash buffer	Concentration	Blocking time (min)
Bovine serum albumin (BSA) fatty acid free, globulin free	1 % (w/v)	30
BSA	2 % (w/v)	30
Chemiblocker	5 % (v/v)	30
Chemiblocker	5 % (v/v)	120
Normal goat serum	5 % (v/v)	30 *
Normal goat serum + BSA	5 % (v/v) + 0.2 % (w/v)	30
Normal goat serum + BSA	5 % (v/v) + 1 % (w/v)	30

After blocking unspecific binding sites blocking buffer was removed and replaced with wash buffer containing appropriately diluted primary antibodies. Primary antibodies were directed against several different epitopes, these are i) the C-terminally HA-tagged Ca$_v$1.3 channel, ii) the N-terminus of native Cav1.3 channel and iii) several other markers to asses overall retinal morphology.

Table 31 List of primary antibodies used in retina immunohistochemistry.

Antibody	Dilution	Company + Order #
Anti-HA High Affinity, Rat monoclonal antibody (clone 3F10)	1:1,000	Roche, 11 867 423 001
Anti-Hemagglutinin, Mouse Monoclonal 16B12, Alexa Fluor Conjugates	1:100	Invitrogen, A21287
Anti-Ca(v)1.3 alpha1 subunit Antibody	1:200	Millipore, ABN11
Anti-Tyrosine Hydroxylase	1:1,000	Millipore, AB152
Rabbit anti-Calbindin D-28k	1:10,000	Swant, CB-38a
Rabbit anti-Calretinin	1:2,500	Swant, 7697

Rabbit anti-Parvalbumin	1:5,000	Swant, PV 25
PMCA1 ATPase Antibody	1:100	ThermoScientific, PA1-914
PKC α Antibody (H-7)	1:500	Santa Cruz Biotechnology, sc-8393

Incubation with primary antibodies typically took place overnight at 4 °C (~ 20 hours). Some sections were not exposed to a primary antibody but served as negative controls to check for unspecific binding of secondary antibodies – these were incubated with wash buffer only.

The next day, primary antibody solutions or wash buffer were discarded and the sections were washed for 10, 20 and 30 minutes with wash buffer. Secondary antibodies were diluted appropriately in wash buffer and were added to each corresponding slide that was incubated with a primary antibody to which the secondary antibody should bind and to the negative control slides. Sections were incubated for 1 hour at room temperature and protected from light.

Table 32 List of secondary antibodies used in retina immunohistochemistry.

Antibody	Dilution	Company + Order #
Alexa Fluor 594 Goat Anti-Rat IgG (H+L)	1:400	Invitrogen, A-11007
Alexa Fluor 488 Goat Anti Rabbit IgG (H+L)	1:400	Invitrogen, A-11008
Alexa Fluor 568 Goat Anti-Mouse IgG (H+L)	1:400	Invitrogen, A-11004

Next, secondary antibodies were discarded and slides were washed for 10, 20 and 30 minutes with wash buffer. Due to the fact that the retina is a light sensitive tissue one should logically assume that sample autofluorescence is a major concern. As a consequence of that, some sections were not exposed to any antibody but were incubated with wash buffer only.

Finally, all sections (1st and 2nd antibodies, negative controls (only 2nd antibody) and autofluorescence controls (no antibodies)) were incubated with DAPI (1:10,000) for 3 minutes. After a last wash step for 3x 10 minutes sections were embedded in AquaPoly/Mount-Gel and coverslips were mounted. The gel was allowed to dry for 1-2 hours at room temperature in the dark, before all slides were stored at 4 °C.

2.7.5. Staining of brain cryo-sections

Sections were air-dried at room temperature for 1-2 hours before being encircled with commercially-available nail-polish to create a reservoir for blocking and antibody solutions. After another 15 minutes of drying sections were washed 3x 20 minutes with wash buffer.

Table 33 Composition of wash buffer used in brain immunohistochemistry.

Substance	Final concentration
Triton X-100	0.4 % (v/v)
NaN$_3$	0.05 % (w/v)
Dissolve in 1x PBS to final 1 l	

All sections were blocked in wash buffer supplemented with 5 % (v/v) normal goat serum and 1 % (w/v) BSA for 1 hour at room temperature. Subsequently, sections were incubated with primary antibodies or wash buffer (i.e. negative control and autofluorescence control) at 4 °C overnight.

Table 34 List of primary antibodies used in brain immunohistochemistry.

Antibody	Dilution	Company + Order #
Anti-HA High Affinity, Rat monoclonal antibody (clone 3F10)	1:1,000	Roche, 11 867 423 001
Anti-Ca(v)1.3 alpha1 subunit Antibody	1:200	Millipore, ABN11

The next day, primary antibody solutions or wash buffer were discarded and the sections were washed 3x 10 minutes with wash buffer. Secondary antibodies were diluted appropriately in wash buffer and were added to each corresponding slide. Incubation took place for 1 hour in the dark at room temperature.

Table 35 List of secondary antibodies used in brain immunohistochemistry.

Antibody	Dilution	Company + Order #
Alexa Fluor 594 Goat Anti-Rat IgG (H+L)	1:400	Invitrogen, A-11007
Alexa Fluor 488 Goat Anti-Rat IgG (H+L)	1:400	Invitrogen, A-11006
Alexa Fluor 488 Goat Anti Rabbit IgG (H+L)	1:400	Invitrogen, A-11008

Secondary antibodies were discarded and slides were washed 3x 10 minutes with wash buffer. All sections were incubated with DAPI (1:10,000) for 3 minutes. After a last wash step for 3x 10 minutes sections were embedded in AquaPoly/Mount-Gel and coverslips were mounted. The gel was allowed to dry for 1-2 hours at room temperature in the dark, before all slides were stored at 4 °C.

2.7.6. Image acquisition and analysis

All fluorescence microscopy images were taken at VetImaging with a Zeiss AxioImager Z2. Exposure times for all respective fluorescence excitation channels were set to equal values to

guarantee comparability among samples. The camera was an AxioCam MRc5. Early immunohistochemistry experiments were analyzed on a Zeiss Axiovert 200M.

For retinae, a 20x objective (20x/0.8 Plan-Apochromat) was used. One set of images was taken with a 40x objective (40x/0.95 Plan-Apochromat). For brains, three objectives with the least magnification were used:

- 5x/0.16 Plan-Neufluar
- 10x/0.3 Plan-Neufluar
- 20x/0.8 Plan-Apochromat

Raw Carl Zeiss images (.czi) were transformed into JPEG files by the Carl Zeiss ZEN 2012 image software (blue edition). Subsequent picture analysis and creation of figures for this work were carried out in Adobe Photoshop CS5 Extended (version 12.0.4) from Adobe Systems, Inc. All images in this work were taken at the Technology Platform VetCore (a core facility at the University of Veterinary Medicine, Vienna, Austria) in collaboration with Dr. Martin Glösmann.

3. Experimental Results

3.1. Control PCR of digested mCaV1.3(1a)-8b-42-HA-pcDNA3 construct

The sequence of this construct was loaded into Serial Cloner (version 2.6.1). The circular DNA molecule had an overall length of 11,817 bp. Virtual cuts with the restriction enzymes described in section 2.1.3. were performed with the program to determine the length of expected PCR products in control digests.

- EcoRI

```
Restriction analysis of mCaV1.3(1a)-8b-42-HA-pcDNA3 [Circular]
Incubated with EcoRI

2 fragments generated.

   1:    8.634 bp  -  From EcoRI[5308]   To  EcoRI[2125]

   2:    3.183 bp  -  From EcoRI[2125]   To  EcoRI[5308]
```

- BglII

```
Restriction analysis of mCaV1.3(1a)-8b-42-HA-pcDNA3 [Circular]
Incubated with BglII

3 fragments generated.

   1:    5.267 bp  -  From BglII[6562]   To  BglII[12]

   2:    4.271 bp  -  From BglII[12]     To  BglII[4283]

   3:    2.279 bp  -  From BglII[4283]   To  BglII[6562]
```

- HindIII

```
Restriction analysis of mCaV1.3(1a)-8b-42-HA-pcDNA3 [Circular]
Incubated with HindIII

2 fragments generated.

   1:   10.533 bp  -  From HindIII[2173] To  HindIII[889]

   2:    1.284 bp  -  From HindIII[889]  To  HindIII[2173]
```

After digestion was carried out PCR products as well as marker and negative controls were loaded onto 1 % (w/v) agarose gels. For electrophoresis conditions refer to section 2.1.3. or the insets in Figure 6.
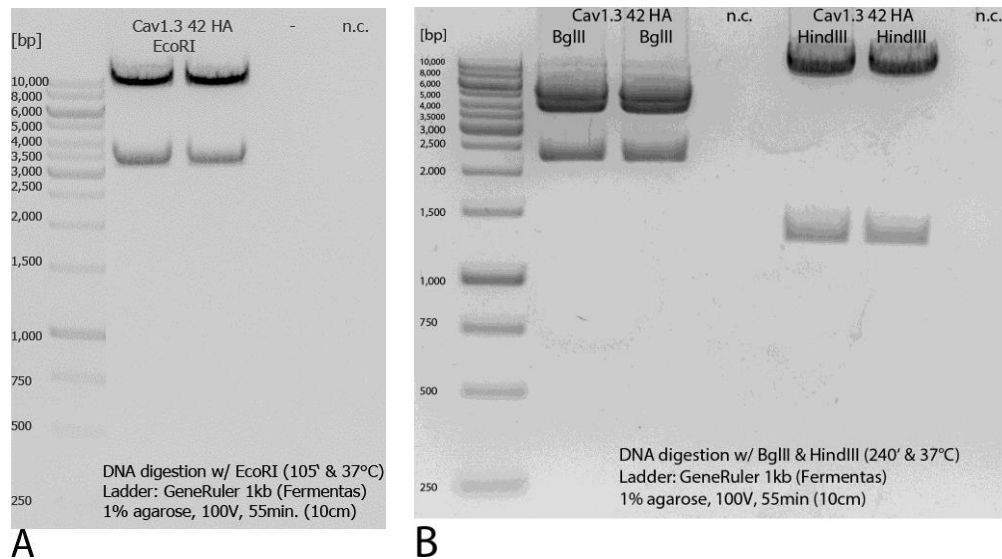
Figure 6 DNA digestion of Ca$_v$1.3-HA plasmid DNA.

One µg µl^{-1} of plasmid DNA was digested with EcoRI, BglII, and HindIII, respectively, and loaded onto a 1 % (w/v) agarose gel. Two restriction digests and its negative control (n.c.) per respective enzyme are shown. (A) Digestion with EcoRI yielded 2 DNA fragments corresponding to predicted sizes (~ 3,100 and ~ 8,600 bp). No signal was detected in the negative control. (B) Restriction digests with BglII and HindIII produced 3 (~ 2,300, ~ 4,200 and ~ 5,200 bp) and 2 (~ 1,200 and ~ 10,500 bp) fragments, respectively, in good agreement with predicted sizes. No signals in both negative controls.

The results from these 3 enzymatic digestions supported the correctness of our Ca$_v$1.3-HA construct which was used in subsequent tsA-201 cell transfection experiments.

3.2. Genotypings of experimental mice

3.2.1. Genotypings of Ca$_v$1.3 DEME

Figure 7 shows an exemplary PCR genotyping loaded onto a 2 % (w/v) agarose gel. C57BL/6N wild-type mice were characterized by one band at 535 bp. Ca$_v$1.3-HA mice showed either 3 bands with 332, 535 and 678 bp (heterozygous) or 332 and 678 bp (homozygous).
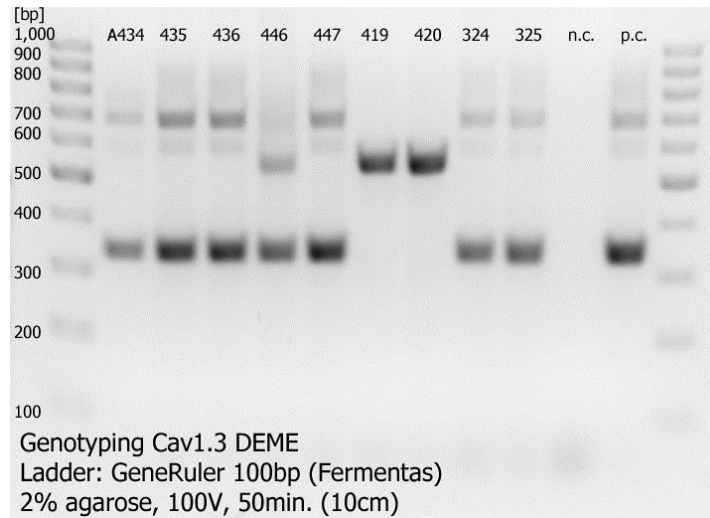
Figure 7 Ca$_v$1.3-HA genotyping

PCR products of mouse tail biopsies were loaded onto a 2 % (w/v) agarose gel (run conditions, see inset). Wild-type mice were characterized by a single band at 535 bp. Heterozygous Ca$_v$1.3 mice were characterized by 3 bands at 332, 535 and 678 bp and homozygous Ca$_v$1.3-HA mice showed 2 bands at 332 and 678 bp. There were no detectable bands in the negative control (n.c.) PCR reaction. A homozygous positive control (p.c.) displayed presence of 3 bands at the corresponding lengths.

Numbers above lanes represent respective mouse identification number.

3.2.2. Genotypings of Ca$_v$1.3 knock-out

Figure 8 shows an exemplary PCR genotyping loaded onto a 1 % (w/v) agarose gel. C57BL/6N wild-type mice were characterized by one band at 300 bp. Ca$_v$1.3 knock-out mice showed either 2 bands with 300 and 450 bp (heterozygous) or a single band at 450 bp (homozygous).
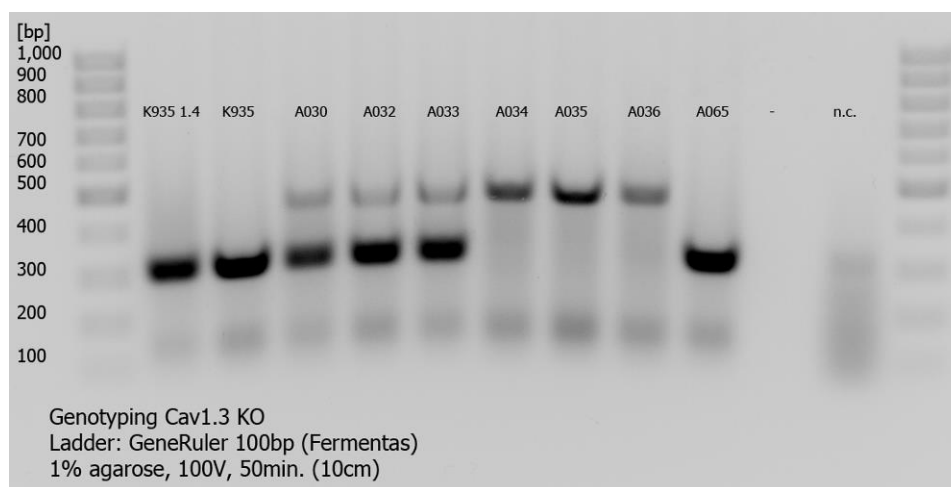
Figure 8 Ca$_v$1.3 knock-out genotyping

PCR products of mouse tail biopsies were loaded onto a 1 % (w/v) agarose gel (run conditions, see inset). Wild-type mice were characterized by a single band at 300 bp. Heterozygous Ca$_v$1.3 knock-out mice were characterized by 2 bands at 300 and 450 bp and homozygous Ca$_v$1.3 knock-out mice showed a single band at 450 bp. There were no detectable bands in the negative control (n.c.) PCR reaction.

Numbers above lanes represent respective mouse identification number.

3.3. Detection of HA-tagged Ca$_v$1.3 in tissue and cell membrane preparations

3.3.1. Immunoblot analysis

Thirty µg of tissue membrane preparations, i.e. retina and brain, and 0.1 µg of transfected cell membrane preparations were loaded onto 6 % polyacrylamide gels. The murine Ca$_v$1.3 channel α1 subunit protein has an approximate size of ~ 247 kDa (Q99246; CAC1D_Mouse; www.uniprot.org). A specific HA signal was seen in both positive controls, i.e. transfected cell membranes (lane 1) and Ca$_v$1.3-HA mouse brain membranes (lane 8). My negative controls, i.e. mock transfected cells and wild-type & Ca$_v$1.3 knock-out mice brain membranes displayed no positive signal in the range of ~ 250 kDa (lanes 2, 7 and 9, respectively).

Retina membrane preparations of homozygous HA-knock-in mice showed an intense HA signal at ~ 250 kDa (lane 5), whereas it was absent in wild-type and Ca$_v$1.3 knock-out animals (lanes 3 and 6, respectively). The fainter signal obtained from heterozygous HA-knock-in mice (lane 4) is, i) a good indicator of accuracy and validity of this experiment and, ii) further supporting the notion of heterozygosity in our genotypings.

To check for equal loading across lanes an antibody against β-tubulin (~ 55 kDa) was used. A signal was absent in transfected cell membrane preparations, possibly due to the fact that only 0.1 µg of proteins were loaded (this was done because 30 µg of proteins yielded a very intense HA signal that reached into the negative control lane, i.e. mock transfected cells). β-tubulin levels were consistent and equal for each respective tissue alone (i.e. retina & brain) but showed a great difference in intensity across both tissues. For a broader interpretation of this phenomenon, please refer to section 4.1.
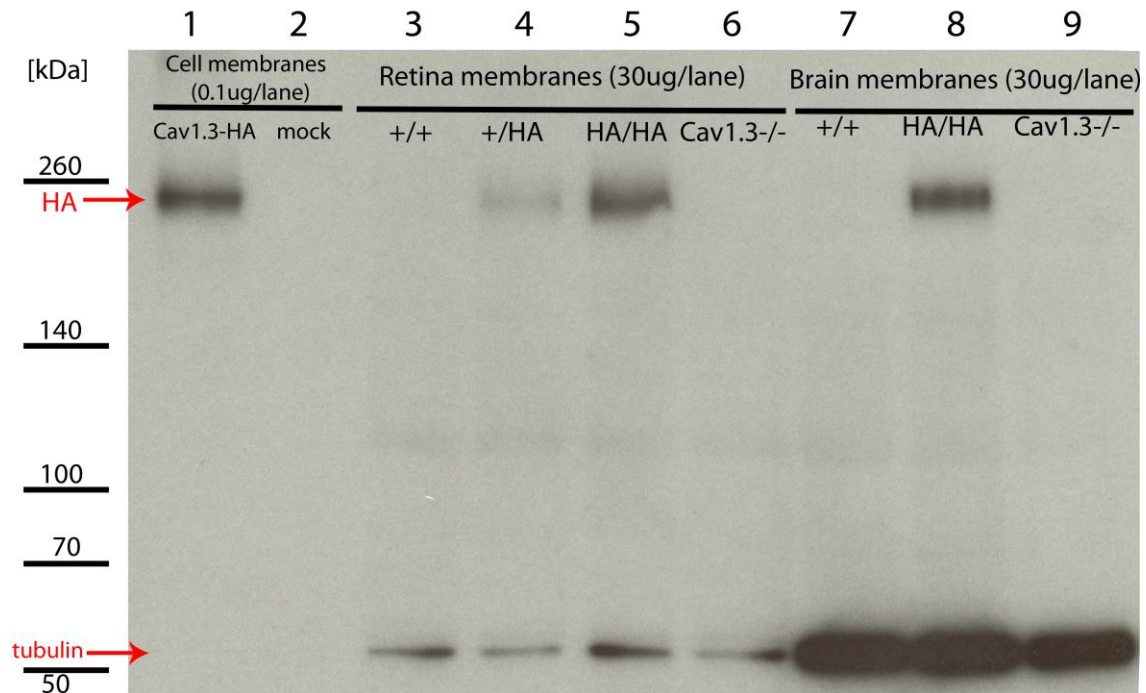
Figure 9 Western Blot of cell, retina and brain membrane preparations.

Thirty µg of tissue membrane preparations and 0.1 µg of cell membrane preparations were loaded onto a 6 % (w/v) polyacrylamide gel and probed with an anti-HA antibody and anti-β-tubulin antibody, respectively. Signals of HRP-conjugated secondary antibodies were visualized by incubation with ECL solution followed by exposure to film. HA-specific signals were detected in lanes 1 (HA-transfected cells), 4 and 5 (retinae from Ca$_v$1.3-HA mice) and 8 (brain from Ca$_v$1.3-HA mice). β-tubulin was distributed equally across every respective tissue, but showed great 'intertissue' variability. For more details see text.

3.3.2. Immunoblot transfer efficiency

As described in section 2.5.2., gels were stained in Coomassie staining solution for 2 hours (during blocking of the nitrocellulose membrane) before being de-stained overnight in distilled water. Below are two representatively stained/de-stained SDS polyacrylamide gels representing three independent membrane preparations which showed a slight retention of larger proteins within the gel. As a consequence of this incomplete protein transfer in conjunction with the subsequent 100 % efficient transfer of the low molecular weight loading control protein (β-tubulin, ~ 55 kDa) it can be argued that the densitometric evaluation was not completely accurate, but somewhat underestimated (see section 4.1.).
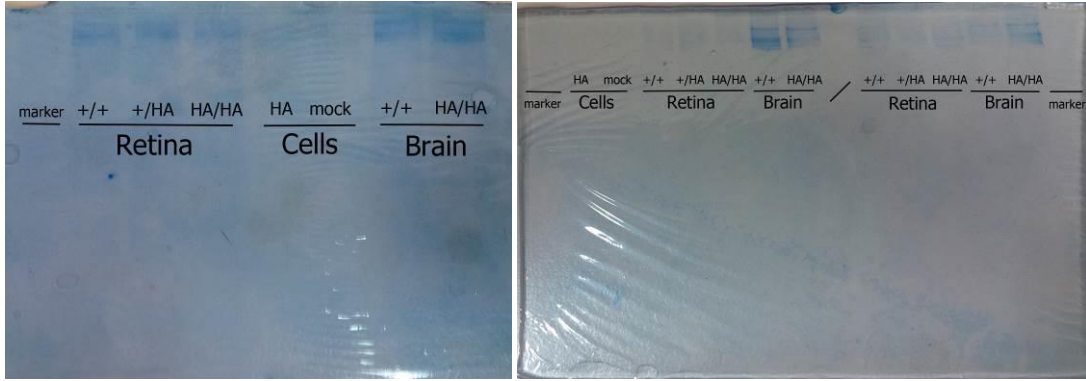
Figure 10 Coomassie staining of polyacrylamide gels.

To check the efficiency of Western Blot transfers polyacrylamide gels were stained in Coomassie solution. After washing with water, retained or residual (large) proteins were visible at the top edge of the gels, whereas low molecular weight proteins were fully transferred onto the nitrocellulose membrane. +/+, wild-type; +/HA, heterozygous; HA/HA, homozygous HA-knock-in.

3.3.3. Statistical analysis

Densitometric and statistical analyses were performed as described in sections 2.5.3. & 2.5.4., respectively.

Peak area under curve (AUC) values were processed in an Excel spreadsheet (Table 36) from which adjusted densities could be inferred. These adjusted densities, represented in arbitrary units (a.u.), were statistically analyzed in GraphPad Prism (Figure 11). Furthermore, standard deviation (SD) and standard error of the mean (SEM) were calculated in Excel to cross-check the results obtained in statistical evaluations.
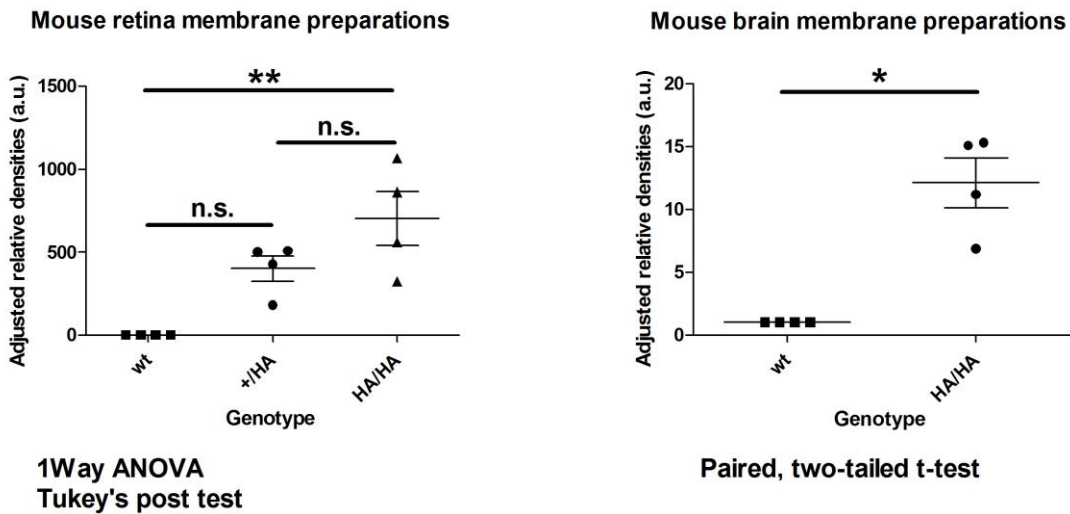
Figure 11 Statistical evaluations based on densitometric analyses of mouse retina and brain membrane preparations.

Adjusted relative densities were calculated in Microsoft Excel. For retina membrane preparations, there was a significant difference between the wild-type and homozygous HA-knock-in mice (P = 0.0034; 99 % confidence interval (CI); One-way ANOVA with Tukey's post test). For brain membrane preparations, there was also a significant difference between the wild-type and homozygous HA-knock-in mice (P = 0.0112; 99 % CI; paired t test). a.u., arbitrary units; n.s., not significant; wt, wild-type; +/HA, heterozygous HA-knock-in; HA/HA, homozygous HA-knock-in; n=4 for all genotypes in both evaluations.

Table 36 Summary of data from densitometric analyses.

β-tubulin retina (29.10.2013)				HA retina (29.10.2013)				adjusted density
sample ID	AUC	rel.density		sample ID	AUC	rel.density		
wt	5.356,7820	1,0000		wt	11,5360	1,0000		1,0000
het	9.425,3380	1,7595		het	10.154,9660	880,2848		500,2997
hom	11.042,6520	2,0614		hom	20.565,0780	1.782,6871		864,7801

β-tubulin brain (29.10.2013)				HA brain (29.10.2013)				adjusted density
sample ID	AUC	rel.density		sample ID	AUC	rel.density		
wt	15.577,0160	1,0000		wt	1.639,5770	1,0000		1,0000
hom	11.906,5300	0,7644		hom	18.902,8860	11,5291		15,0833

β-tubulin retina (04.11.2013)				HA retina (04.11.2013)				adjusted density
sample ID	AUC	rel.density		sample ID	AUC	rel.density		
wt	6.130,7820	1,0000		wt	16,5360	1,0000		1,0000
het	5.639,5480	0,9199		het	6.489,3380	392,4370		426,6203
hom	6.712,6400	1,0949		hom	19.312,1080	1.167,8827		1.066,6495

β-tubulin brain (04.11.2013)				HA brain (04.11.2013)				adjusted density
sample ID	AUC	rel.density		sample ID	AUC	rel.density		
wt	11.656.288,0000	1,0000		wt	1.129,5360	1,0000		1,0000
hom	11.671.924,0000	1,0013		hom	17.295,0870	15,3117		15,2912

β-tubulin retina (29.11.2013)				HA retina (29.11.2013)				adjusted density
sample ID	AUC	rel.density		sample ID	AUC	rel.density		

sample ID	AUC	rel.density		sample ID	AUC	rel.density		adjusted density
wt	9.118,3380	1,0000		wt	59,6070	1,0000		1,0000
het	6.683,9740	0,7330		het	7.819,8230	131,1897		178,9701
hom	10.599,9950	1,1625		hom	22.609,9570	379,3171		326,2966

β-tubulin brain (29.11.2013)				HA brain (29.11.2013)				adjusted density
sample ID	AUC	rel.density		sample ID	AUC	rel.density		
wt	9.290,8030	1,0000		wt	1.964,3050	1,0000		1,0000
hom	12.549,2880	1,3507		hom	18.238,8150	9,2851		6,8742

β-tubulin retina (06.03.2014)				HA retina (06.03.2014)				adjusted density
sample ID	AUC	rel.density		sample ID	AUC	rel.density		
wt	780,4060	1,0000		wt	7,3640	1,0000		1,0000
het	346,7990	0,4444		het	1659,8410	225,3994		507,2190
hom	2877,8410	3,6876		hom	15228,3970	2067,9518		560,7822

β-tubulin brain (06.03.2014)				HA brain (06.03.2014)				adjusted density
sample ID	AUC	rel.density		sample ID	AUC	rel.density		
wt	5654,0330	1,0000		wt	35,7780	1,0000		1,0000
hom	8370,1040	1,4804		hom	592,9910	16,5742		11,1959

	mean	sd	sem	n
wt retina	1,0000	0	0	4
het retina	403,2773	153,921855	76,9609276	4
hom retina	704,6271	326,871312	163,435656	4
wt brain	1,0000	0	0	4
hom brain	12,1111	3,96691721	1,9834586	4

3.4. Immunocytochemical Analysis

Transfected, fixed and stained tsA-201 cells were analyzed by fluorescence microscopy on an AxioImager Z2 microscope (Carl Zeiss Microscopy). All images were taken at VetImaging, a core facility of the University of Veterinary Medicine, Vienna, Austria.

Figure 12 shows one out of 5 independent staining experiments employing an anti-HA antibody (Roche, 1:1,000). A clear HA signal (red, Figure 12 A'), on both the cell membrane and the cytoplasm, could be seen. Mock transfected cells, however, gave no HA-specific signal (Figure 12 B'). These results were supportive of successful transfection and specificity of the anti-HA antibody in immunofluorescence experiments.

DAPI staining (1:10,000) was used to localize cells and control for abnormal cell/nuclear morphology. As can be seen in panels A & B, no malformation of nuclei was visible.
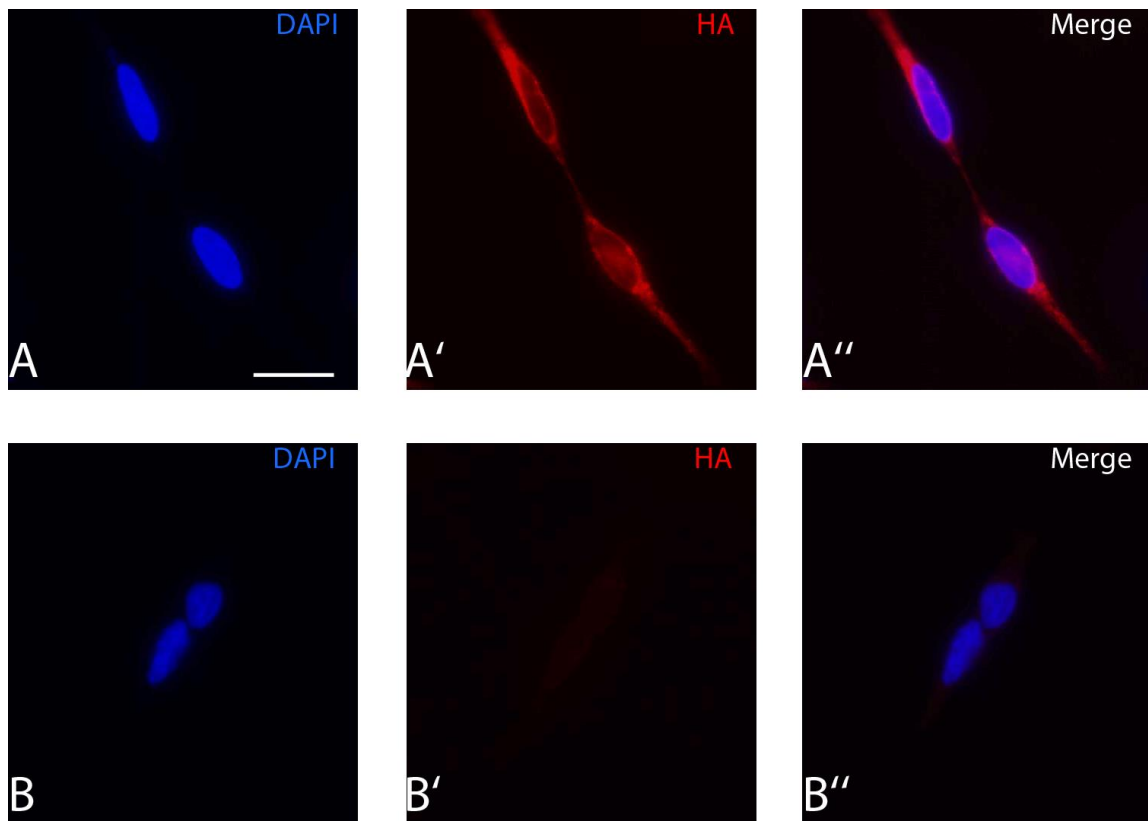
Figure 12 Immunofluorescence microscopy images of transfected tsA-201 cells.

Cells were transfected with $Ca_v1.3$-HA (A, A' & A'') or without, i.e. mock-transfected (B, B' & B''), and stained with an anti-HA antibody and DAPI. DAPI staining was used to localize cells and control nuclear morphology. As seen in panels A and B there was no obvious difference between nuclei. $Ca_v1.3$-HA transfected cells (A') gave a clear membrane and cytoplasmic signal, whereas there was no specific staining in mock transfected cells (B'). Scale bar: 20 µm. N=5.

Both negative control fluorescence images from $Ca_v1.3$-HA or mock transfected cells gave no signal when exposed to a wavelength in the range of the Alexa Fluor 594 fluorophore (Figure 13 A' & B'). This is to support that unspecific binding of the secondary antibody was not present. Furthermore, it provided confirmation that the HA-specific signal in Fig. 12 A' was derived from specific binding of the primary antibody. DAPI staining revealed the position of cells in Figure 13. Signal intensity was equal and no nuclear abnormalities were observable at this magnification.
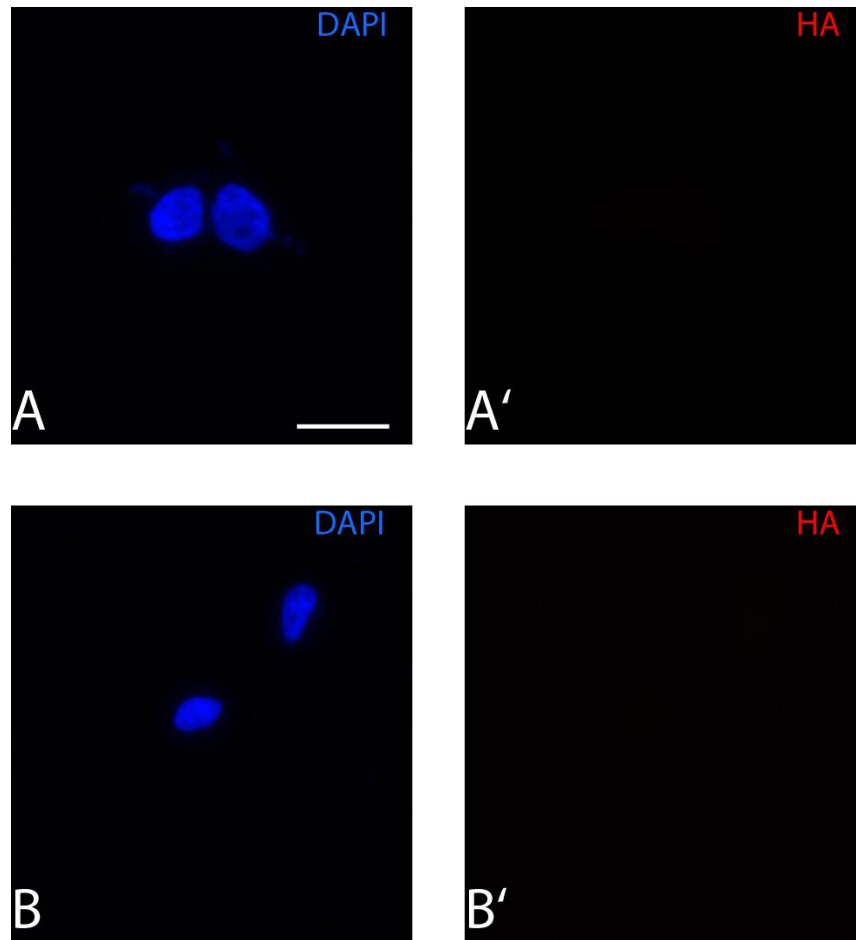
Figure 13 Immunofluorescence microscopy images of transfected tsA-201 cells.

$Ca_v1.3$-HA transfected cells (A, A') and mock transfected cells (B, B') were stained with DAPI. Primary antibody, i.e. anti-HA antibody, was omitted to check unspecific binding of the secondary antibody. DAPI staining was used to localize cells and control nuclear morphology. As seen in panels A and B there was no obvious difference between nuclei. Our secondary antibody (Alexa Fluor 594 Goat Anti-Rat) did not show unspecific labeling (A' and B'). Scale bar: 20 μm. N=5.

3.5. Retina Immunohistochemical Analysis

All retina cryo-sections were treated according to my standard protocol (see Tables 27 and 30). HA-stainings (Section 3.4.3.) were treated differently. My main aims were i) localization of HA-specific $Ca_v1.3$, and ii) elucidating (by various marker proteins) if our genetically modified mice bear any structural alterations in the retina.

3.5.1. Assessment of retinal layer thickness

4',6-diamidino-2-phenylindole, more commonly known as DAPI, binds DNA and can be employed as a highly selective marker for nuclei. By performing DAPI co-stainings I wanted to determine if there are differences in the thickness of all three nuclear layers in the retina, i.e. outer nuclear layer, inner nuclear layer & ganglion cell layer (for an overview see also Figure 4).

Visual inspection of the 3 images in Figure 14 revealed no obvious difference in retinal layer thickness. These data were reproducible over at least 3 independent experiments. Furthermore, nuclei counts revealed no statistically significant changes in outer or inner retinal layer thickness across genotypes (Figure 15).
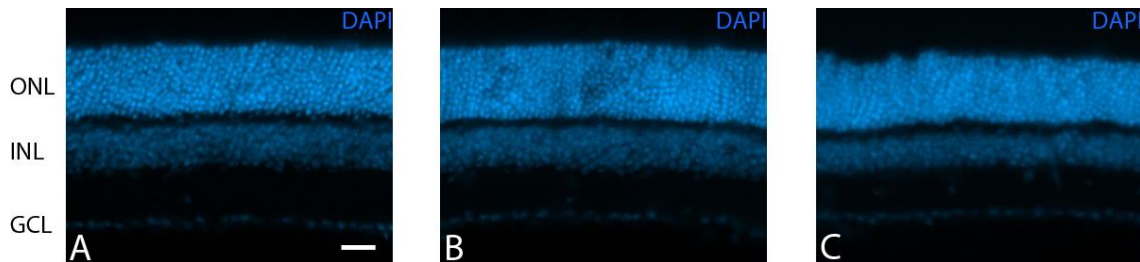
Figure 14 DAPI staining to control retinal layer thickness.

Wild-type (A), $Ca_v1.3$-HA (B) and $Ca_v1.3$ knock-out (C) retina cryo-sections were stained with DAPI to check the thickness of all three nuclear layers, i.e. outer nuclear layer (ONL), inner nuclear layer (INL) and ganglion cell layer (GCL). As can be seen by visual inspection there was no obvious difference in the thickness of either nuclear layer. Scale bar: 20 µm. N=3.
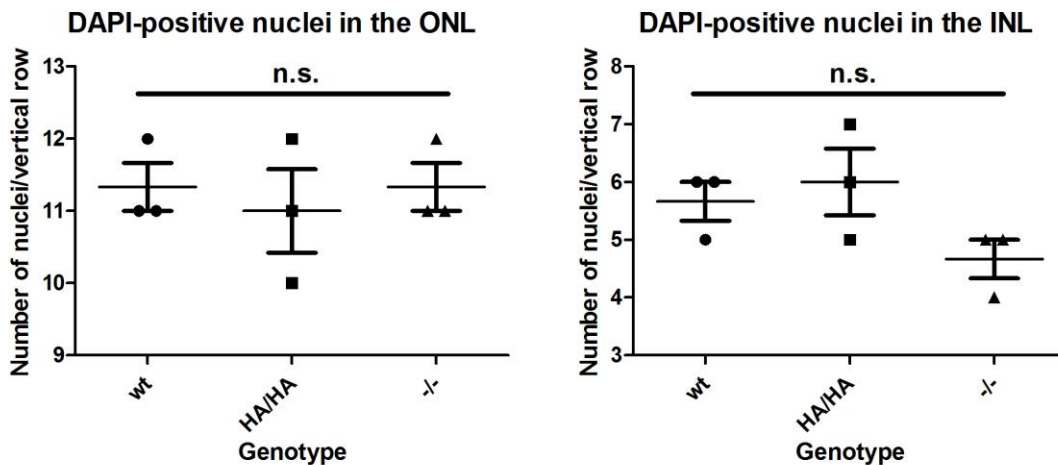
Figure 15 Statistical evaluations of outer and inner nuclear layer thicknesses based on nuclei counts.

Nuclei per vertical row of wild-type (wt), Ca$_v$1.3-HA (HA/HA) and Ca$_v$1.3 knock-out (-/-) retina cryo-sections were counted in Adobe Photoshop and ZEN and statistically evaluated in GraphPad Prism. No statistically significant change in retinal layer thickness could be observed, based on the test method used. One-way ANOVA with Tukey's post test (99 % CI). ONL, outer nuclear layer; INL, inner nuclear layer; n.s., not significant; wt, wild-type; HA/HA, homozygous HA-knock-in; -/- homozygous Ca$_v$1.3-knock-out. N=3.

3.5.2. Assessment of inner retinal morphology

3.5.2.1. Assessment of rod bipolar cells

Protein kinase C alpha (PKC α) is a common marker used to stain and visualize rod bipolar cells (RBPCs) and some amacrine cells in the retina (*53*). By performing immunohistochemistry experiments I investigated if, i) insertion of the HA-tag into the DCRD of the Ca$_v$1.3 α1 subunit, and, ii) a complete knock-out of the Ca$_v$1.3 channel, confers any morphological change in RBPCs as compared to C57BL/6N wild-type mice.

Visual inspection of Figure 16 revealed no obvious change in RBPC number and/or morphology between wild-type (A), Ca$_v$1.3-HA (B) or Ca$_v$1.3$^{-/-}$ (C) retinae. This observation was reproducible over 3 independent experiments for A and B, and over 2 independent experiments for C.
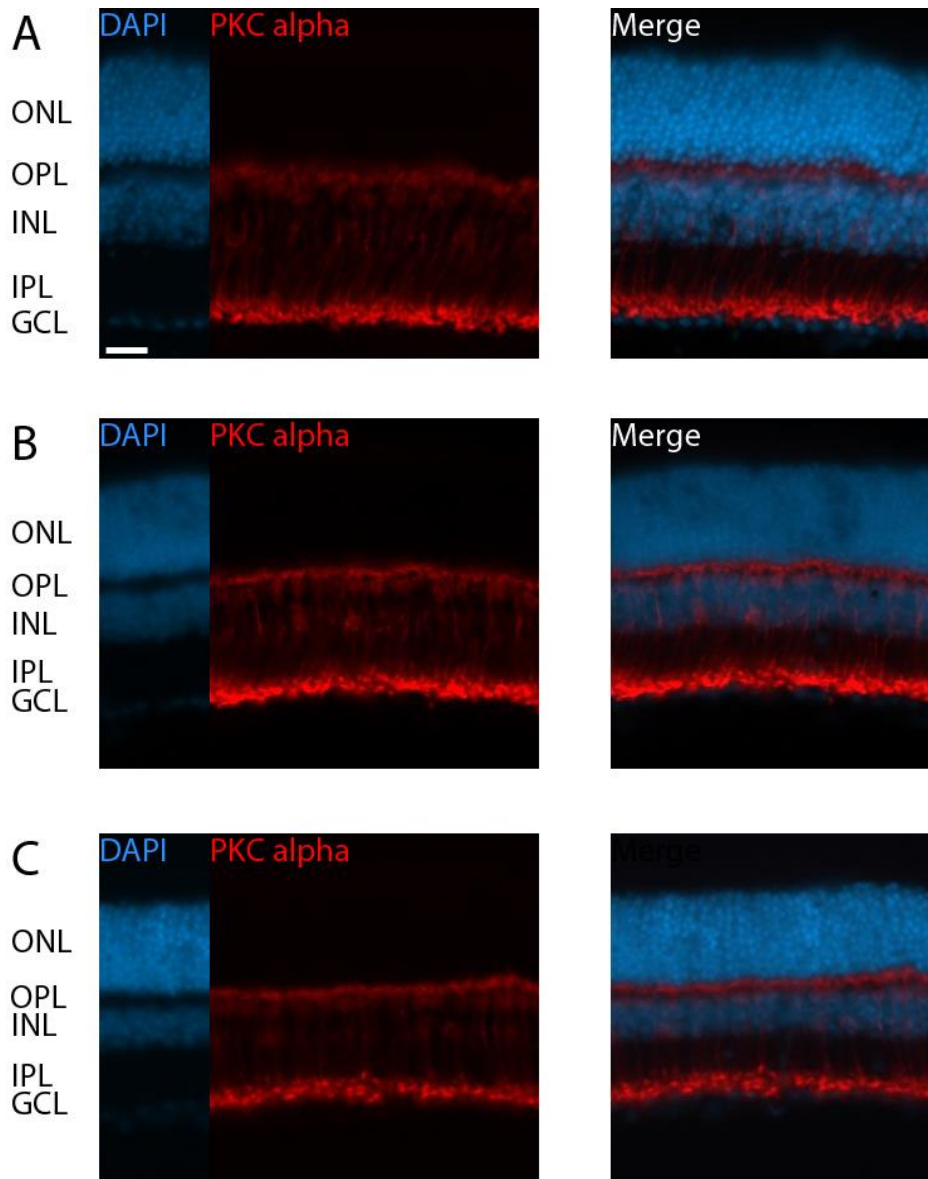
Figure 16 PKC α immunofluorescence microscopy images of retina cryo-sections.

Wild-type (A), Ca$_v$1.3-HA (B) and Ca$_v$1.3 knock-out (C) retina cryo-sections were stained with an anti-PKC α antibody and DAPI. No apparent changes in rod bipolar cell number and/or morphology could be observed. Scale bar: 20 µm. N=3 for A and B, N=2 for C.

3.5.2.2. Assessment of Calbindin-positive cells

Calbindin is a calcium binding protein that is commonly employed as a marker for several types in the retina. It is present in cell bodies, dendrites and axons of horizontal cells, as well as in amacrine cells at the inner edge of the INL, displaced amacrine cells in the GCL and ganglion

cells. The IPL is composed of 5 strata, of which 3 are prominently labeled by Calbindin, highlighting the contribution of amacrine cell dendrites to this layer (*53*).

The outer band, i.e. strata 1-2, contains processes from OFF amacrine cells while the center band, i.e. strata 2-3, separates the OFF sublamina (outer) from the ON sublamina (inner, strata 4-5) (*23*).

Staining with an anti-Calbindin antibody revealed no apparent changes across genotypes in terms of cell number or distribution across the retina (Figure 17). Stratification of the IPL was intact in each genotype. It should be noted here that the Ca_v1.3-HA retina cryo-section (B) is slightly smaller than the wild-type (A) and the Ca_v1.3 knock-out (C). Based on retinal layer thickness calculations (see Figures 14 and 15), however, I conclude that this might be due to the fact that the slide containing Ca_v1.3-HA cryo-sections was taken from a more distally located region of the retina (in terms of proximity to the optic nerve).
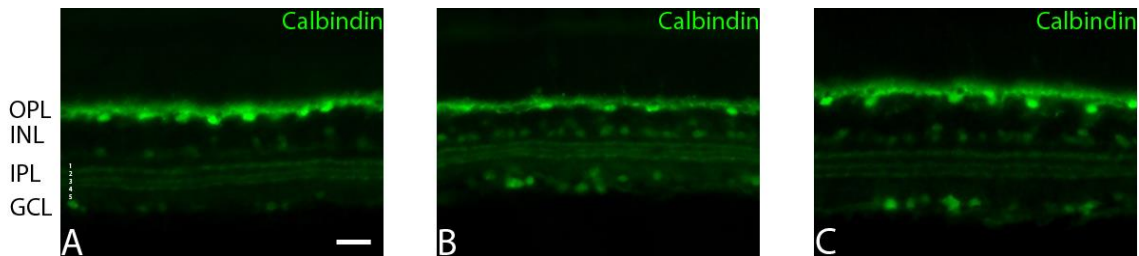
Figure 17 Calbindin immunofluorescence microscopy images of retina cryo-sections.

Wild-type (A), Ca_v1.3-HA (B) and Ca_v1.3 knock-out (C) retina cryo-sections were stained with an anti-Calbindin antibody. No apparent changes in terms of cell number or distribution could be observed. Stratification of the IPL is still intact. Scale bar: 20 µm. N=2.

3.5.2.3. Assesment of Calretinin-positive cells

Calretinin is another calcium binding protein and a commonly used marker. It is present in amacrine cells, displaced amacrine cells and ganglion cells. Furthermore, specific staining of 3 strata in the IPL was observed (*53*). In fact, Calretinin and Calbindin double staining experiments revealed that they are found in the same strata in the IPL (*23*).

Consequently, staining with Calretinin (Figure 18) also revealed no obvious changes between wild-type (A), Ca_v1.3-HA (B) or Ca_v1.3$^{-/-}$ (C) in terms of actively labeled cells and/or their respective distribution across the inner retina. Stratification of the IPL is still intact.
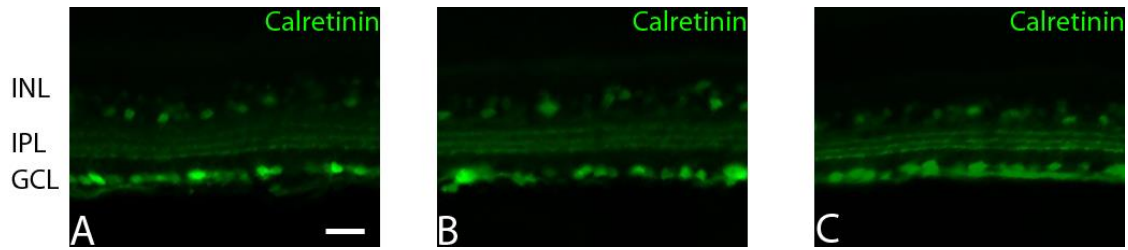
Figure 18 Calretinin immunofluorescence microscopy images of retina cryo-sections.

Wild-type (A), Ca$_v$1.3-HA (B) and Ca$_v$1.3 knock-out (C) retina cryo-sections were stained with an anti-Calretinin antibody. No apparent changes in terms of cell number or distribution could be observed. Stratification of the IPL is still intact. Scale bar: 20 µm. N=3 for A and B, N=2 for C.

3.5.2.4. Assessment of retinal Ca^{2+} extrusion via PMCA1

As mentioned in section 1.1., cells possess several extrusion mechanisms to restore the physiological [Ca^{2+}]$_i$. Plasma membrane Ca^{2+}-ATPases, of which there are four isoforms, PMCA1-4, are involved in this process. The PMCA1 isoform was investigated in this study.

It was shown that PMCA1 is prominently expressed in rod and cone photoreceptor terminals in the OPL, weakly in horizontal cells and moderately in OFF and ON cone bipolar cells in the INL. Also, OFF and ON cone bipolar cell terminals were labeled in both sublaminae of the IPL (*54*). Cav1.3 channels have been reported to be expressed together but non-overlapping with PMCA1 within the photoreceptor terminals in tree shrew retina (*55*). This finding prompted us to investigate potential differences in PMCA1 expression in Cav1.3$^{-/-}$ retinae.

As obvious from Figure 19, PMCA1 staining was prominent in the inner retina. There was strong labeling in the OPL, moderate labeling in the INL and moderately strong labeling in the IPL. This is in good agreement with (*54*) and was observable in all three genotypes (wild-type (A), Ca$_v$1.3-HA (B) and Ca$_v$1.3$^{-/-}$ (C)). However, there were several PMCA1 immunoreactive puncta in the outer retina (arrows), just below the photoreceptor inner segments of the Ca$_v$1.3 knock-out animal (C).
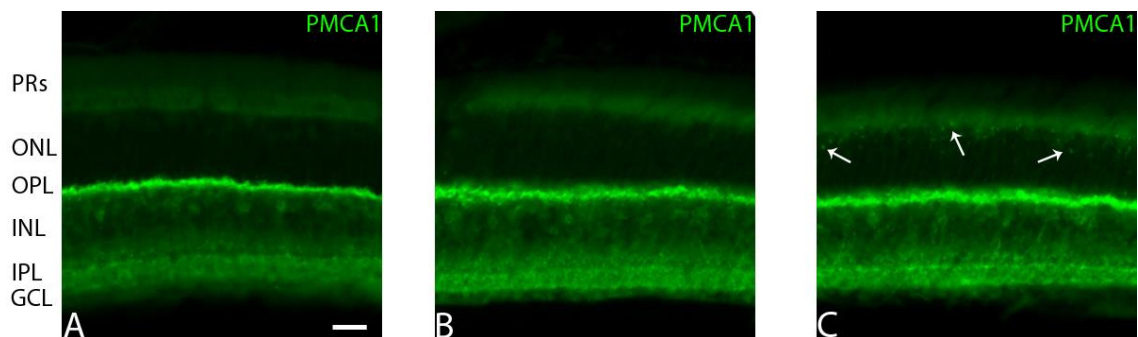

**Figure 19 PMCA1 immunofluorescence microscopy images of retina cryo-sections.**

Wild-type (A), Ca$_v$1.3-HA (B) and Ca$_v$1.3 knock-out (C) retina cryo-sections were stained with an anti-PMCA1 antibody. There was no apparent difference between genotypes in PMCA1 staining of the inner retina. However, several PMCA1 immunoreactive puncta (arrows) in the INL were observed in the Ca$_v$1.3$^{-/-}$ mouse (C). Scale bar: 20 µm. N=2.

Figure 20 highlights PMCA1 immunoreactive puncta in the knock-out animal (C), visualized at a higher magnification (40x) and compared to the wild-type (A) and Ca$_v$1.3-HA (B). These puncta are mostly located in the upper part of the ONL, close to PR inner segments (red arrowheads). Some puncta were localized more internally (white arrowhead).
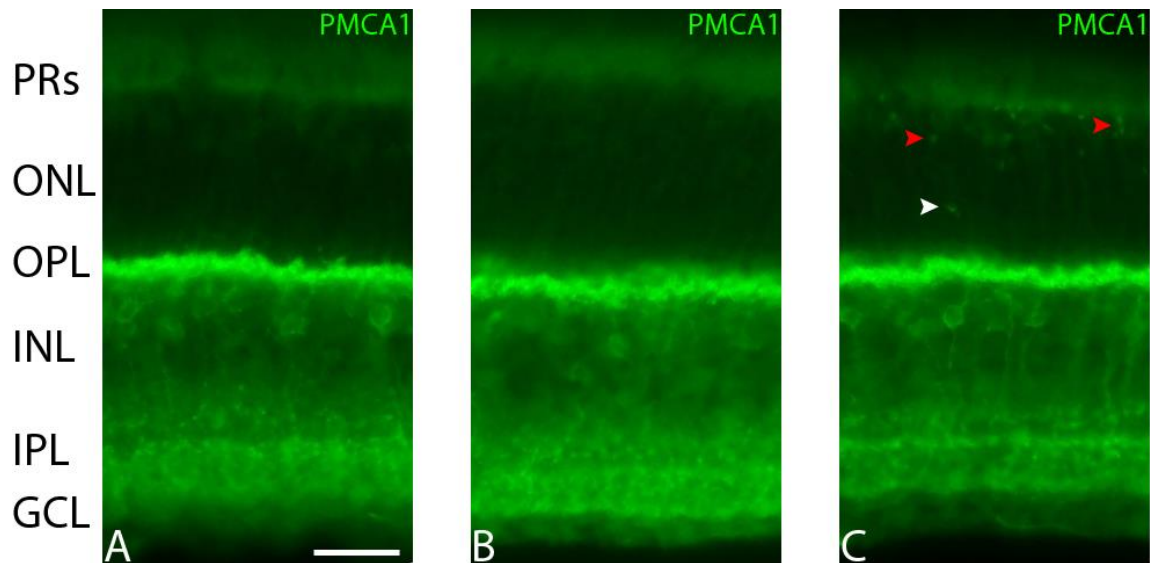
Figure 20 PMCA1 immunofluorescence microscopy images of retina cryo-sections at higher magnification (40x).

Wild-type (A), Ca$_v$1.3-HA (B) and Ca$_v$1.3 knock-out (C) retina cryo-sections were stained with an anti-PMCA1 antibody and visualized at a higher magnification. Again, there was no difference in PMCA1 staining of the inner retina between genotypes. PMCA1 immunoreactive puncta (red and white arrowheads) were observed throughout the ONL in the Ca$_v$1.3$^{-/-}$ mouse (C). Scale bar: 20 µm. N=2.

3.5.2.5. Assessment of Parvalbumin-positive cells

Parvalbumin is another calcium binding protein and serves as a marker protein as well. Studies have highlighted its distribution in amacrine cells and ganglion cells (*53*), and amacrine cell processes have been shown to extend into the IPL whereas displaced amacrine cells are present in the GCL (*56*).

My Parvalbumin stainings (Figure 21) showed only weak labeling of amacrine cells in the INL but prominent labeling of cells in the GCL, which is in good agreement with (*56*). However, no

exact distinction between displaced amacrine cells and ganglion cells in the GCL could be made. Based on the generally weak labeling of (displaced) amacrine cells and the strong labeling of ganglion cells (56), however, I suppose that most cells in the GCL are in fact ganglion cells. No significant difference between wild-type (A), Ca$_v$1.3-HA (B) or Ca$_v$1.3$^{-/-}$ (C) was observed.
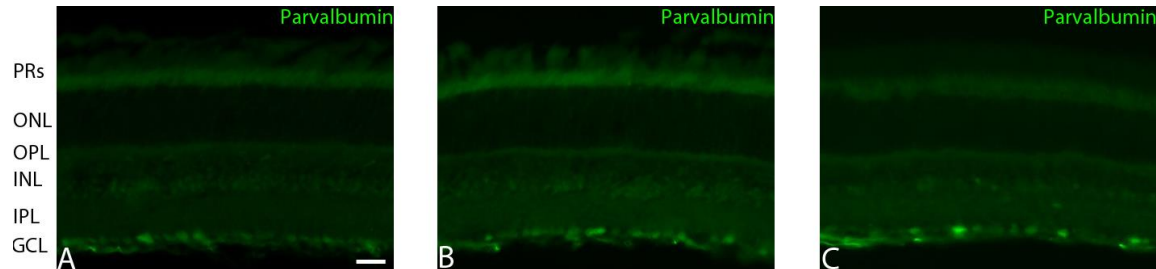
Figure 21 Parvalbumin immunofluorescence microscopy images of retina cryo-sections.

Wild-type (A), Cav1.3-HA (B) and Cav1.3 knock-out (C) retina cryo-sections were stained with an anti-Parvalbumin antibody. There was prominent labeling of ganglion cells in the GCL, and, possibly, some displaced amacrine cells, whereas there was very weak labeling of amacrine cells in the INL. No apparent changes in terms of immunoreactivity of cells or distribution in respective layers could be observed, however. Scale bar: 20 μm. N=3 for A and B, N=2 for C.

3.5.2.6. Assessment of Tyrosine Hydroxylase-positive cells

Tyrosine hydroxylase is an oxygenase catalyzing the hydroxylation of the amino acid tyrosine into L-DOPA (L-3,4-dihydroxyphenylalanine) which is in turn a precursor for dopamine, an important neurotransmitter in the CNS. Dopaminergic cells in the mouse retina were shown to be amacrine cells (based on their immunoreactivity toward anti-tyrosine hydroxylase antibodies) (53).

My Tyrosine hydroxylase (TH) stainings showed strong reactivity of a small number of amacrine cells in the inner nuclear layer (Figure 22). However, no abnormalities in terms of number, morphology or distribution across all three genotypes (wild-type (A), Ca$_v$1.3-HA (B) and Ca$_v$1.3$^{-/-}$ (C)) could be observed.
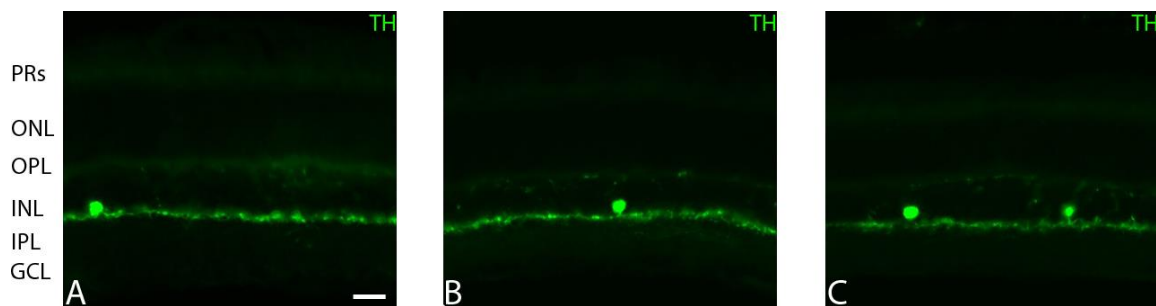
Figure 22 Tyrosine hydroxylase (TH) immunofluorescence microscopy images of retina cryo-sections.

Wild-type (A), Ca$_v$1.3-HA (B) and Ca$_v$1.3 knock-out (C) retina cryo-sections were stained with an anti-Tyrosine hydroxylase (TH) antibody. According to (*53*), amacrine cells in the INL are strongly labeled. However, no change in cell number across genotypes could be observed. Scale bar: 20 µm. N=3 for A and B, N=2 for C.

3.5.3. HA stainings

As shown in Figure 9, detection of HA-tagged Cav1.3 in Western blot analyses was quite straight forward. To establish HA-specific staining in retina immunohistochemistry experiments cryo-sections of wild-type (panels B, B' and B'') and Ca$_v$1.3-HA (panels A, A' and A'') mouse retinae were treated under different experimental conditions. As obvious from Figure 23 it was difficult to obtain an HA-specific signal.

In the first case (panels A & B), cryo-sections were treated according to a common protocol, i.e. fixation for 15 minutes with 4 % (w/v) PFA, washing with 1x PBS + 0.1 % (v/v) Triton X-100 and blocking with 1 % (w/v) BSA for 30 minutes. For these initial experiments, I employed an anti-HA antibody directly conjugated with the Alexa Fluor 488 fluorophore (Invitrogen). Immunofluorescence images of Ca$_v$1.3-HA cryo-sections revealed labeling in the INL and the GCL (Figure 23 A). However, the same staining pattern could also be observed in the wild-type negative control (Figure 23 B). Such staining problems were observable over 2 independent experiments. Moreover, IF images of transfected tsA-201 cells revealed unspecific labeling of this antibody in mock transfected cells (data not shown).

Cryo-sections in panels A' and B' were fixed with 2 % (w/v) PFA for 10 minutes, washed with 1x PBS + 0.2 % (v/v) Triton X-100 and blocked with 5 % (v/v) normal goat serum (NGS) for 30 minutes. No specific HA signal with a rat monoclonal anti-HA antibody from Roche was observed. This antibody was shown to bind specifically to the HA epitope in immunocytochemistry experiments (see Figure 12).

Panels A'' and B'' show cryo-sections that were treated as in A' and B' but exposed to heat induced antigen retrieval. Sections were incubated in ~ 100 °C hot citrate buffer pH 6.0 for 20 minutes. However, also this treatment, with the reasoning to lessen protein crosslinks and consequently expose the masked HA epitope, showed no increase in HA-specificity.

Note that panels A', A'', B' and B'' were color enhanced to observe possible HA- signals. This intense background is not derived from the secondary antibody (see also Figure 27).
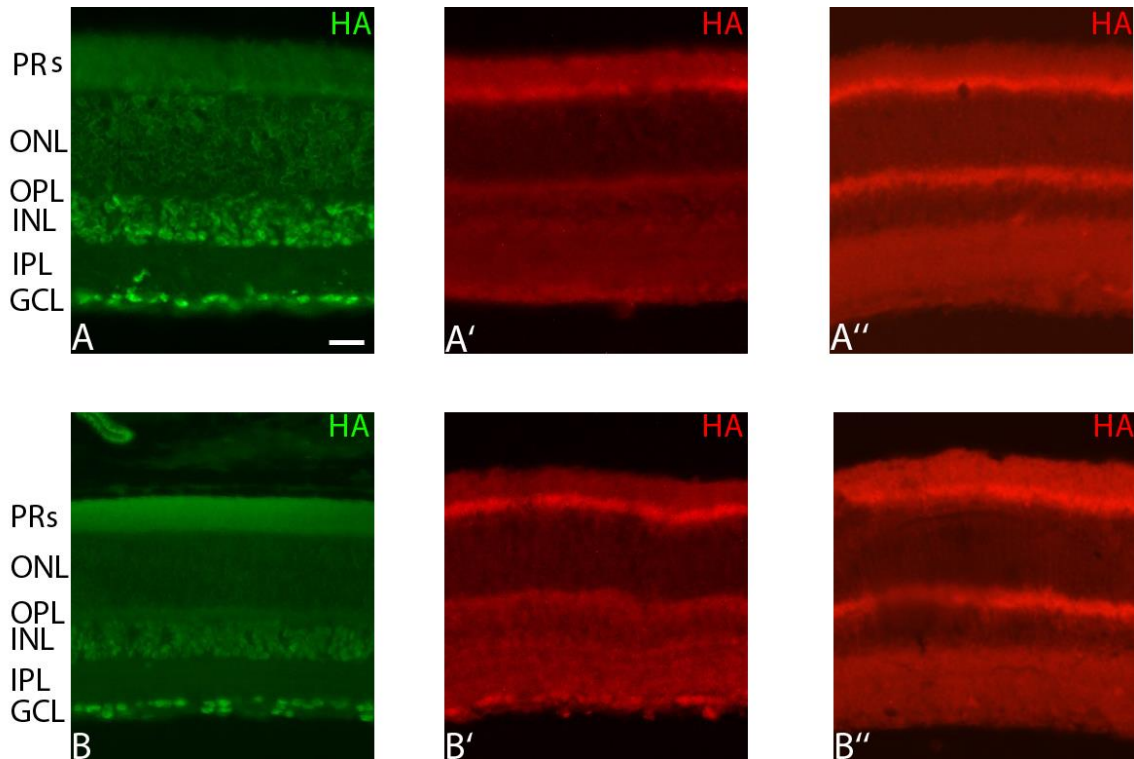
Figure 23 HA immunofluorescence microscopy images of retina cryo-sections.

Ca$_v$1.3-HA (A, A' & A'') and C57BL/6N wild-type (B, B' & B'') retina cryo-sections were treated with different immunohistochemistry parameters (fixative, fixation time, wash buffer, blocking reagent and different anti-HA antibodies) to develop specific HA stainings.

A & B. Retina cryo-sections were fixed with 4 % (w/v) PFA for 15 minutes, washed with 1x PBS supplemented with 0.1 % (v/v) Triton X-100 and blocked with 1 % (w/v) BSA for 30 minutes. Staining with a directly labeled mouse monoclonal anti-HA antibody from invitrogen.

A' & B'. Cryo-sections were fixed with 2 % (w/v) PFA for 10 minutes, washed with 1x PBS supplemented with 0.2 % (v/v) Triton X-100 and blocked with 5 % (v/v) normal goat serum for 30 minutes. Staining with a monoclonal anti-HA antibody from Roche.

A'' & B''. Same conditions as in A' & B' but with heat induced antigen retrieval, i.e. exposure to ~ 100 °C hot citrate buffer pH 6.0. Same antibody as in A' & B'.

Scale bar: 20 µm. N=2 for A & B and A' & B'. N=1 for A'' & B''.

3.5.4. Ca$_v$1.3 stainings

Staining of wild-type and Ca$_v$1.3 knock-out retina cryo-sections with an anti-Ca$_v$1.3 antibody revealed no specific staining (Figure 24). Rather, the staining pattern between wild-type (A) and Ca$_v$1.3 knock-out (B) was virtually the same.
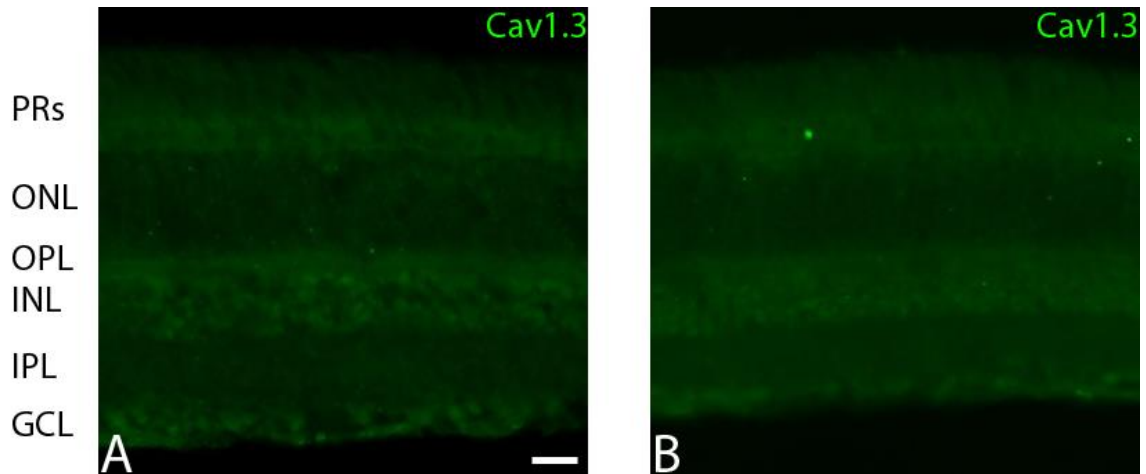
Figure 24 Ca$_v$1.3 immunofluorescence microscopy images of retina cryo-sections.

Wild-type (A) and Ca$_v$1.3 knock-out (B) retina cryo-sections were stained with an anti-Ca$_v$1.3 antibody. No specific Ca$_v$1.3 staining could be obtained, as seen by equal signal intensity between the wild-type and Ca$_v$1.3 knock-out. Scale bar: 20 µm. N=2.

3.5.5. Negative and autofluorescence controls

3.5.5.1. Anti-Mouse 2nd antibody (Alexa Fluor 568)

Exposing retina cryo-sections only to the secondary antibody (goat anti-mouse coupled to Alexa Fluor 568) revealed no unspecific labeling of cells (Figure 25).
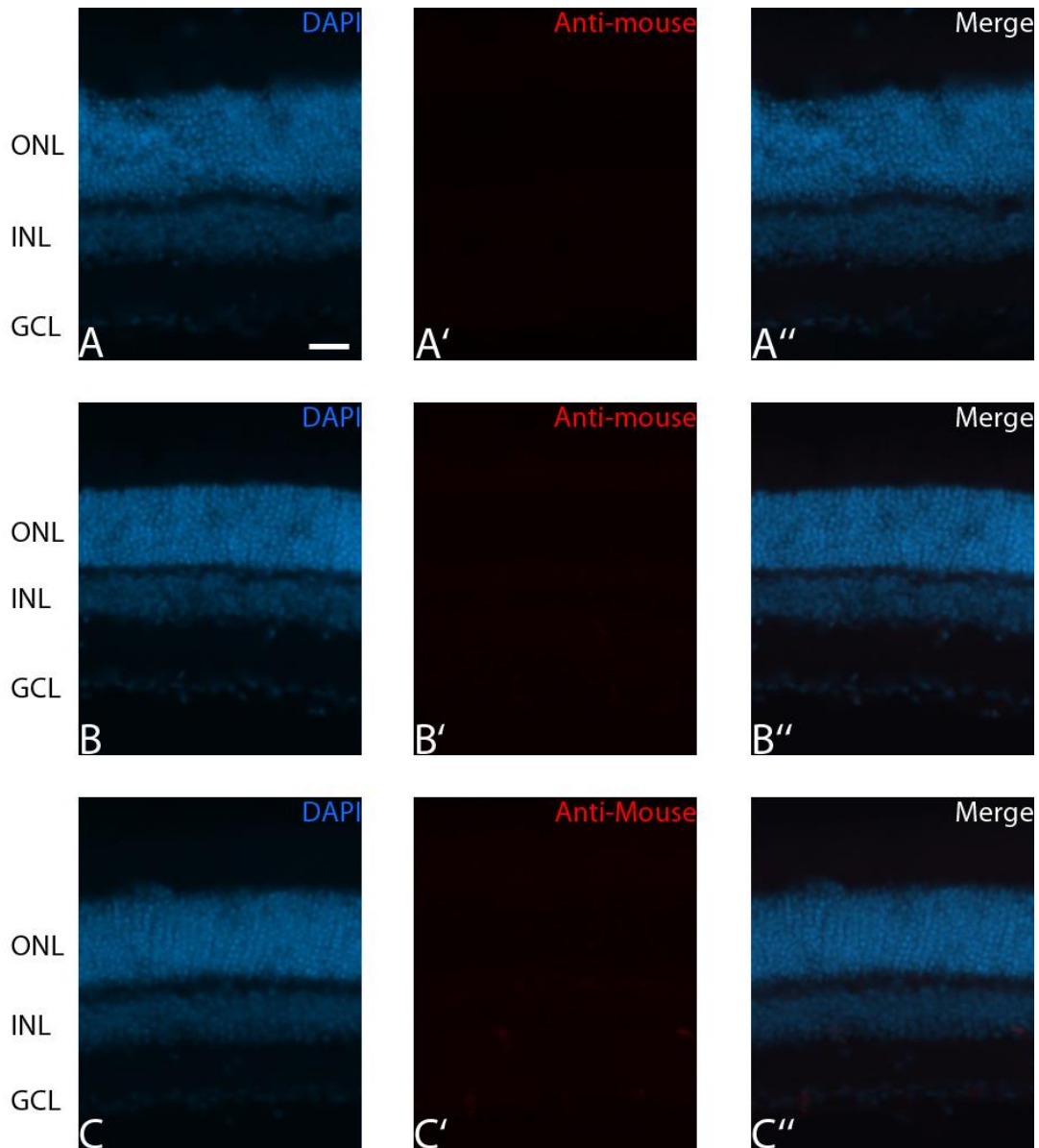
Figure 25 Goat anti-mouse negative control immunofluorescence microscopy images of retina cryo-sections.

Wild-type (A, A' & A''), Ca$_v$1.3-HA (B, B' & B'') and Ca$_v$1.3 knock-out (C, C' & C'') retina cryo-sections were exposed only the secondary antibody (goat anti-mouse coupled to Alexa Fluor 568) and co-stained with DAPI. There was no unspecific labeling of the 2nd antibody. Scale bar: 20 μm. N=3.

3.5.5.2. Anti-Rabbit 2nd antibody (Alexa Fluor 488)

Exposing retina cryo-sections only to the secondary antibody (goat anti-rabbit coupled to Alexa Fluor 488) revealed no unspecific labeling of cells but minor fluorescence could be seen when excited with a 488 nm laser line (Figure 26). However, as demonstrated in my autofluorescence controls (Figure 28), this was due to tissue autofluorescence – especially in the green channel – as fluorescence intensity in autofluorescence controls and negative controls were virtually the same.
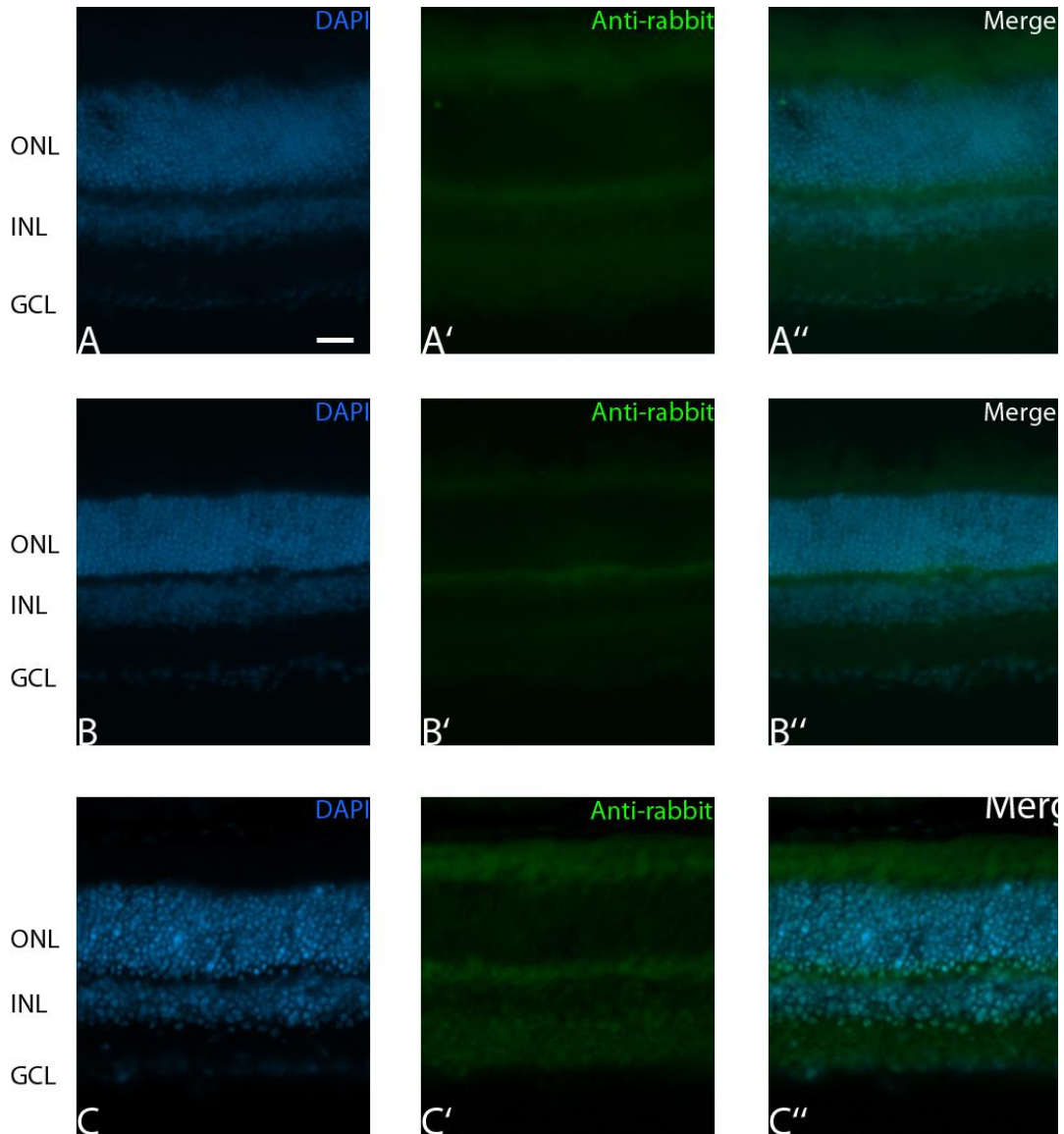

Figure 26 Goat anti-rabbit negative control immunofluorescence microscopy images of retina cryo-sections.

Wild-type (A, A' & A''), Ca$_v$1.3-HA (B, B' & B'') and Ca$_v$1.3 knock-out (C, C' & C'') retina cryo-sections were exposed only the secondary antibody (goat anti-rabbit coupled to Alexa Fluor 488) and co-stained with DAPI. Minor autofluorescence could be seen in the green (eGFP) channel. Scale bar: 20 µm. N=3.

3.5.5.3. Anti-Rat 2nd antibody (Alexa Fluor 594)

Exposing retina cryo-sections only to the secondary antibody (goat anti-rat coupled to Alexa Fluor 594) revealed no unspecific labeling of cells (Figure 27).
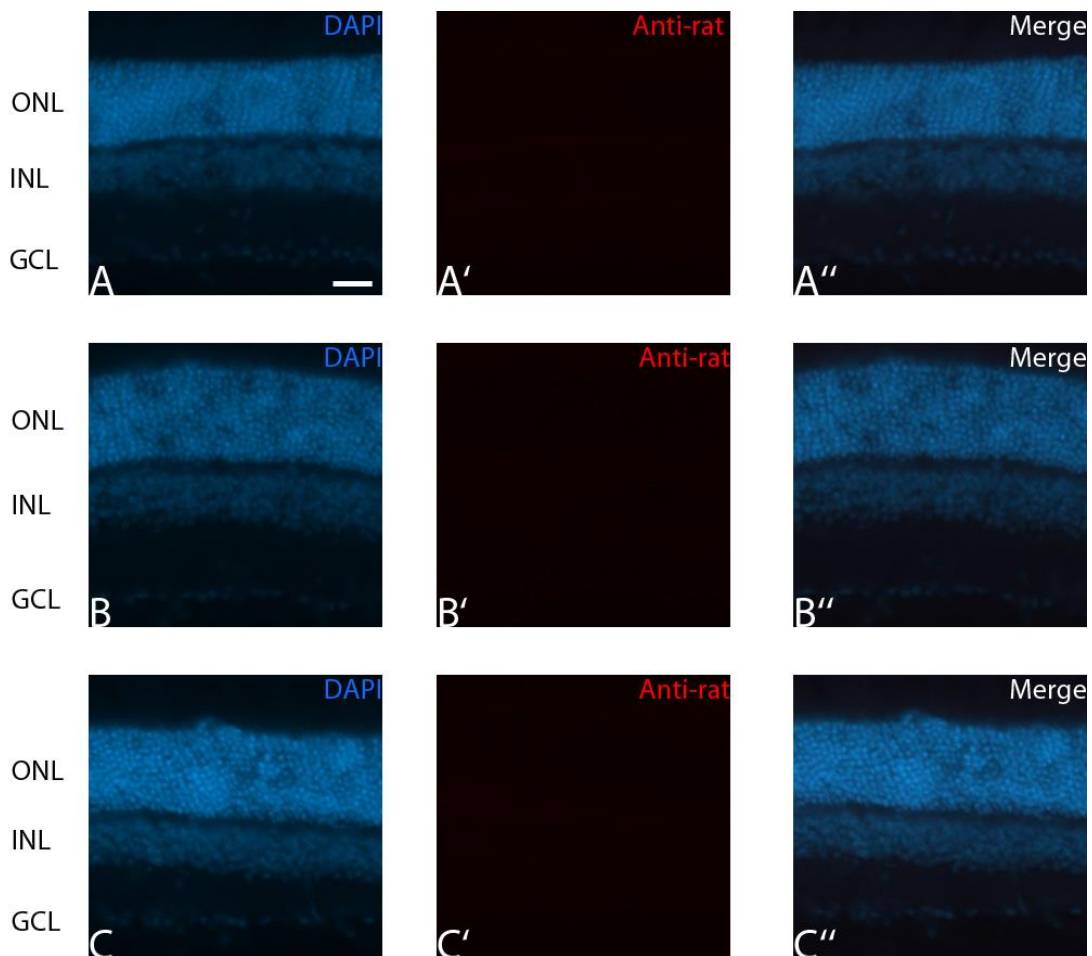
Figure 27 Goat anti-rat negative control immunofluorescence microscopy images of retina cryo-sections.

Wild-type (A, A' & A''), Ca$_v$1.3-HA (B, B' & B'') and Ca$_v$1.3 knock-out (C, C' & C'') retina cryo-sections were exposed only the secondary antibody (goat anti-rat coupled to Alexa Fluor 594) and co-stained with DAPI. There was no unspecific labeling of the 2nd antibody. Scale bar: 20 µm. N=3.

3.5.5.4. Autofluorescence

Retina cryo-sections were solely stained with DAPI but without any antibodies to check tissue autofluorescence. Fixation with paraformaldehyde introduces protein crosslinks to maintain tissue morphology but it can also be a source of autofluorescence as aldehydes are known to generate fluorescent products. Another important aspect rendering it necessary to check for autofluorescence is the tissue itself, more specifically the substances within (*57*). It is widely known that the retina – as a photoreactive tissue – produces a great deal of autofluorescence. Therefore, it is necessary to control if the obtained signal in immunofluorescence experiments is indeed specific and not derived from autofluorescence of the specimen.

Retina cryo-sections were excited with 3 filter sets, i.e. DAPI, eGFP and Texas Red to check for autofluorescence in the range of all secondary antibodies (goat anti-rabbit Alexa Fluor 488, goat anti-mouse Alexa Fluor 568 and goat anti-rat Alexa Fluor 594). As evident in Figure 28 there was only minor autofluorescence in the eGFP channel (A', B' & C'), corroborating the notion that the signal obtained in negative control experiments with the goat anti-rabbit Alexa Fluor 488 secondary antibody was due to autofluorescence from the tissue and not derived from the antibody. There was no tissue autofluorescence when excited through the Texas Red channel (A'', B'' & C'').
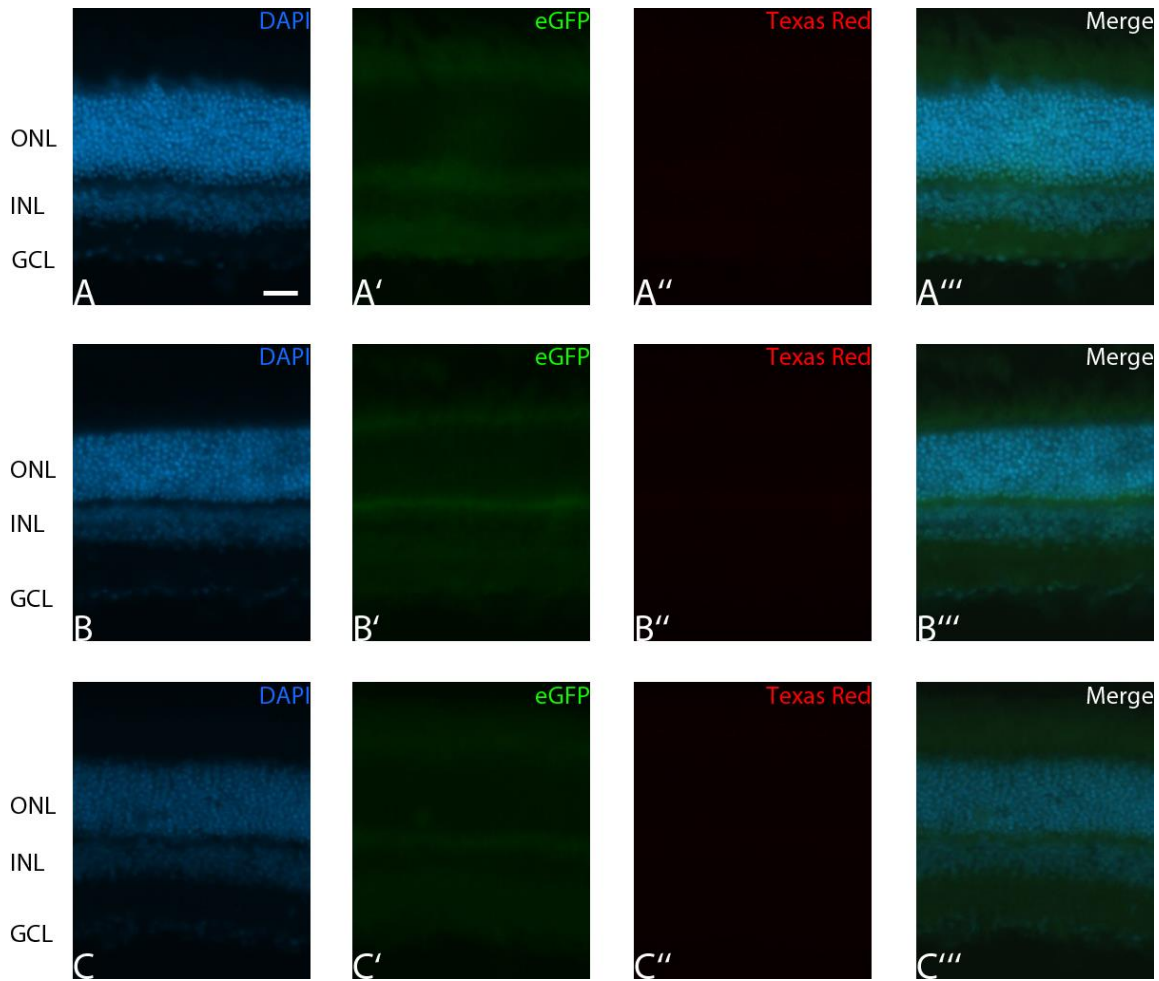
Figure 28 Autofluorescence control immunofluorescence microscopy images of retina cryo-sections.

Wild-type (A, A', A'' & A'''), Ca$_v$1.3-HA (B, B', B'' & B''') and Ca$_v$1.3 knock-out (C, C', C'' & C''') retina cryo-sections were stained with DAPI and excited through all 3 filter sets corresponding to the wavelengths of all secondary antibodies. Minor tissue autofluorescence was detectable only through the green (eGFP) channel. Scale bar: 20 µm. N=3.

3.6. Brain Immunohistochemical Analysis

To test if both antibodies show the same specificity problems as in the retina I decided to stain brain cryo-sections. A recent study highlighted the presence of *CACNA1D* mRNA in the hippocampus and cerebellum (*35*). On the protein level, Ca$_v$1.3 has been shown to be present in the cerebellum, mostly in Purkinje cells but also in the granular and molecular layers (*58*) while in the hippocampus Ca$_v$1.3 has been found in the dentate gyrus and the CA1 and CA3 regions (*59*).

The cerebellum is located at the posterior end of the brain and appears as a separate structure. Therefore, it is easily accessible in posterior cryo-sectioning experiments and coronal sections can be adhered to glass slides within seconds. The hippocampus is a structure located beneath the cerebral cortex. In coronal cryo-sectioning, it is protected by the above lying cerebrum and complete hippocampal sections can be taken onto glass slides. Based on recent observations that Cav1.3 is present in these regions and the easy access in cryo-sectioning experiments described above, I focused on both brain structures. Negative and autofluorescence control experiments revealed no unspecific labeling by secondary antibodies or tissue autofluorescence, respectively (data not shown).

3.6.1. Hippocampus

Staining mouse brain cryo-sections containing the hippocampus and dentate gyrus with an anti-HA antibody (Roche; 1:1,000) revealed no specific labeling of cells (Figure 29). This trend was observable over two independent experiments.
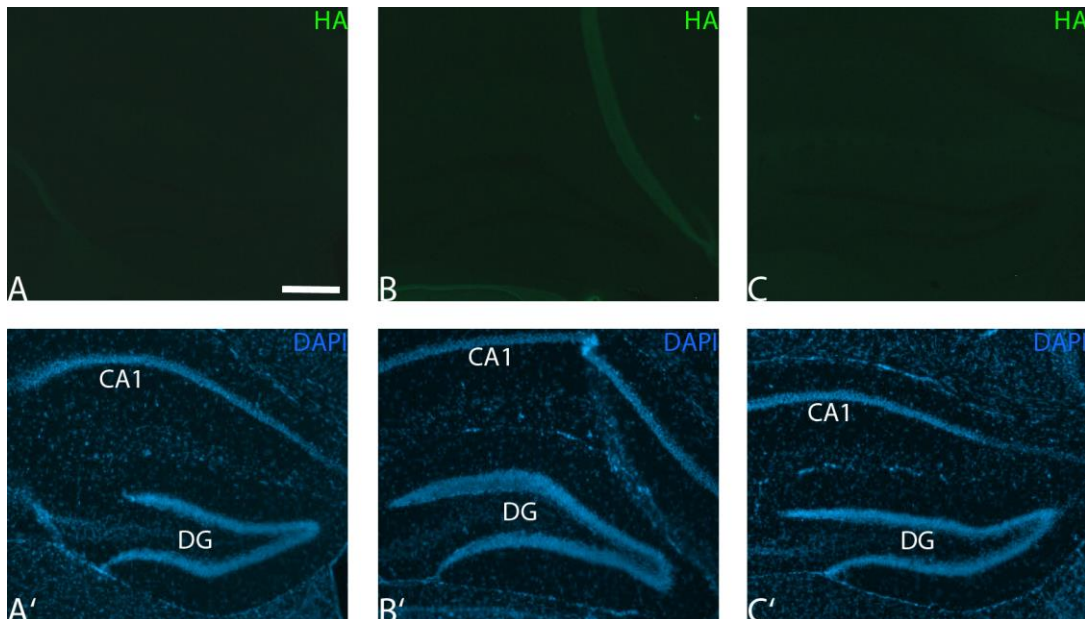

Figure 29 HA immunofluorescence microscopy images of brain cryo-sections.

Wild-type (A, A'), Ca$_v$1.3-HA (B, B') and Ca$_v$1.3 knock-out (C, C') brain cryo-sections were stained with an anti-HA antibody and DAPI. DAPI staining was used to localize the dentate gyrus (labeled structure in the bottom half of A', B' and C', respectively). There was no HA-specific staining in the Ca$_v$1.3-HA genotype (B). DG, dentate gyrus; CA1, cornu ammonis 1 region of the hippocampus. Scale bar: 200 µm. N=2.

Staining hippocampus cryo-sections with my anti-Ca$_v$1.3 antibody (Millipore; 1:200) revealed rather prominent staining in the wild-type (Figure 30 A) as compared to Ca$_v$1.3-HA or the knock-out (Figure 30 B & C, respectively). This became also evident when I examined the hippocampal CA1 region at a higher magnification, i.e. 20x (Figure 31).
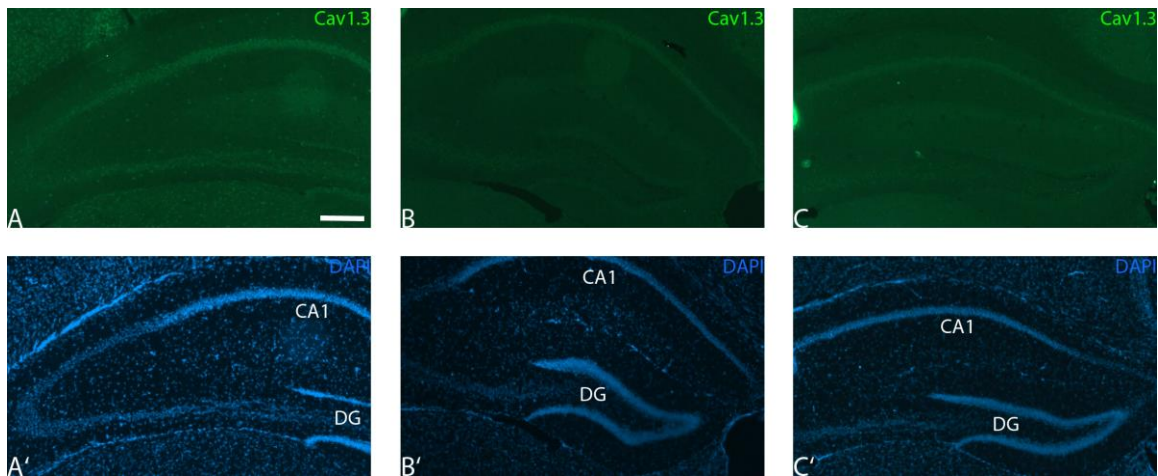
**Figure 30 Ca$_v$1.3 immunofluorescence microscopy images of brain cryo-sections.**

Wild-type (A, A'), Ca$_v$1.3-HA (B, B') and Ca$_v$1.3 knock-out (C, C') brain cryo-sections were stained with an anti-Ca$_v$1.3 antibody and DAPI. DAPI staining was used to localize the hippocampal region. Ca$_v$1.3-specific staining was slightly detectable in the wild-type (A) but less discernable in Ca$_v$1.3-HA (B) or the knock-out (C). DG, dentate gyrus; CA1, cornu ammonis 1 region of the hippocampus. Scale bar: 200 µm. N=2.
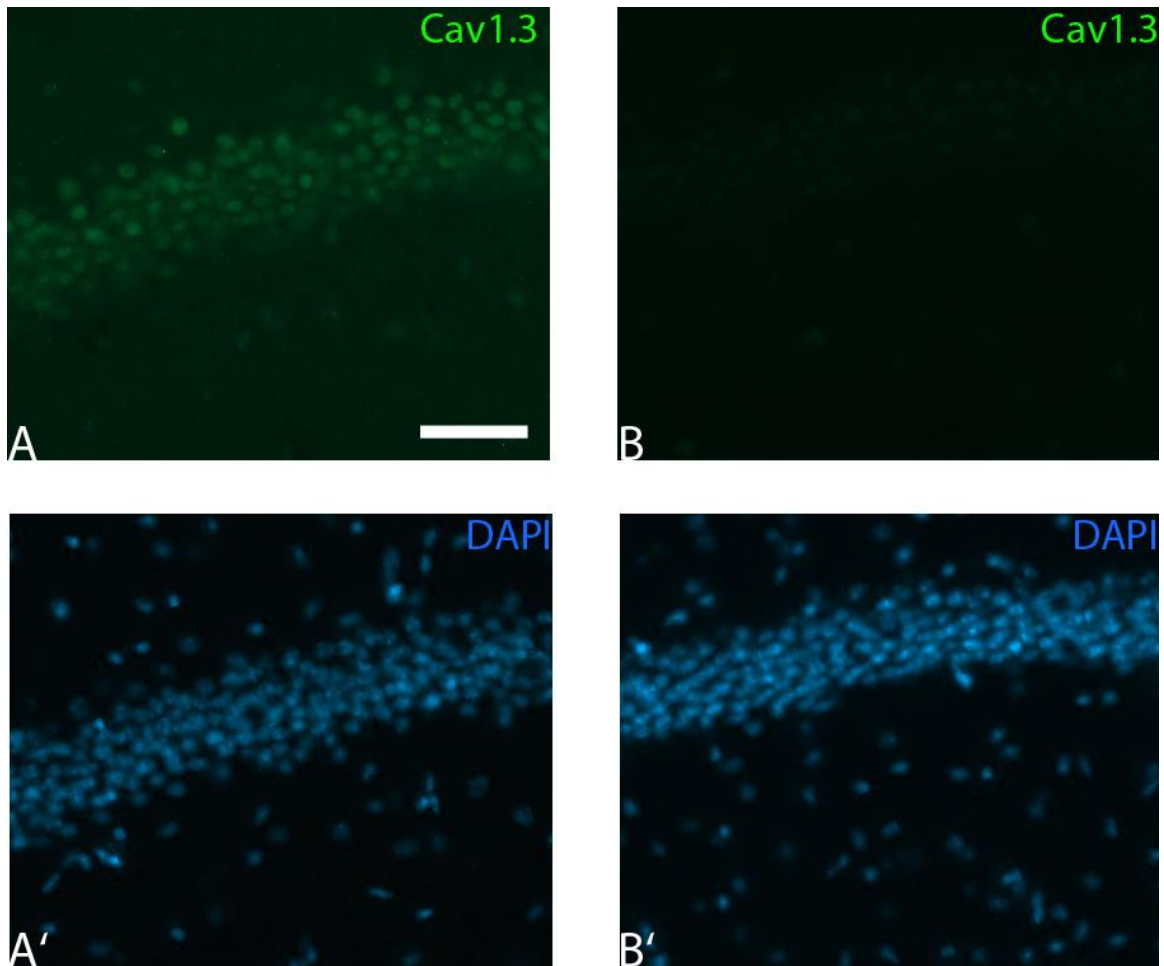
Figure 31 Ca$_v$1.3 immunofluorescence microscopy images of brain cryo-sections at higher magnification (20x)

Wild-type (A, A') and Ca$_v$1.3 knock-out (B, B') brain cryo-sections were stained with an anti-Ca$_v$1.3 antibody and DAPI. DAPI staining was used to localize the hippocampal CA1 region. Ca$_v$1.3-specific staining was present in the wild-type CA1 region (A) but absent in the knock-out (B). Scale bar: 50 µm. N=2.

3.6.2. Cerebellum

Mouse brain cryo-sections containing the cerebellum were stained with my anti-HA antibody (Roche; 1:1,000). No specific labeling of cells could be observed (data not shown). This trend was seen across two biological replicates.

Staining cryo-sections with my anti-Ca$_v$1.3 antibody (Millipore; 1:200) revealed, so far, variable results (Figure 32). While I always observed cell- and process-specific labeling, i.e. granule cells, Purkinje cells and processes in the molecular layer, in the wild-type and Ca$_v$1.3-HA mice, the picture in the knock-out is less clear. In my first biological replicate there was no signal detectable in the Ca$_v$1.3$^{-/-}$ mouse (Figure 32 C). The second replicate, however, revealed staining

in large Purkinje cells and some processes in the molecular layer, whereas granule cells are not immunoreactive (Figure 32 D).
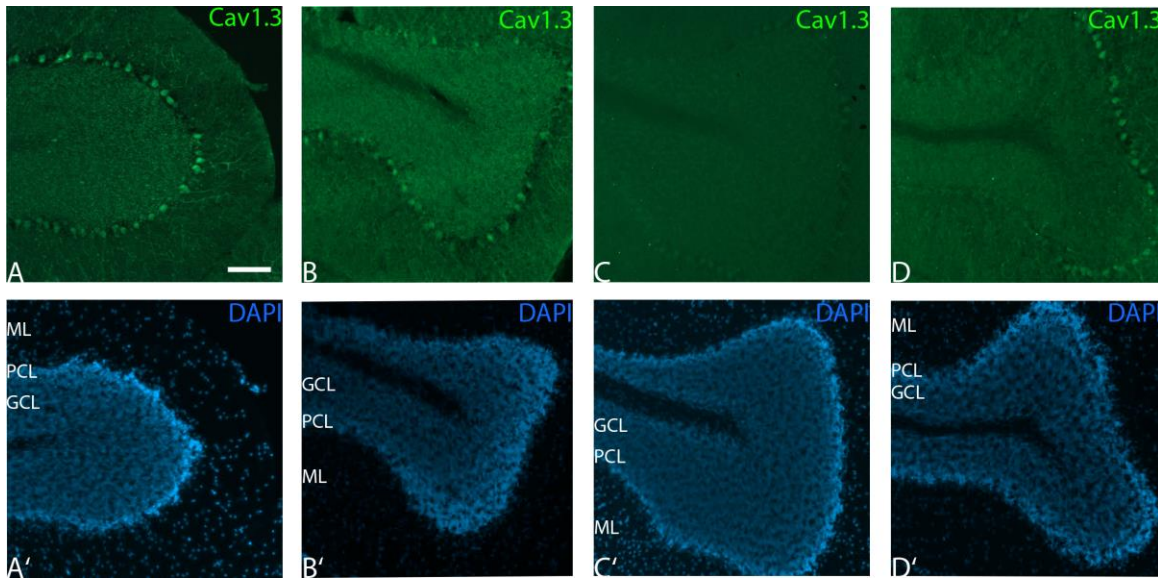
Figure 32 Ca$_v$1.3 immunofluorescence microscopy images of brain cryo-sections.

Wild-type (A, A'), Ca$_v$1.3-HA (B, B') and Ca$_v$1.3 knock-out (C, C', D, D') brain cryo-sections were stained with an anti-Ca$_v$1.3 antibody and DAPI. Ca$_v$1.3-specific signals were detectable in wild-type (A) and Ca$_v$1.3-HA (B) cerebellar cryo-sections. One out of two biological replicates of the Ca$_v$1.3 knock-out gave no specific signals (C) while another most prominently stained large Purkinje cells and processes in the molecular layer (D). GCL, granule cell layer; PCL, Purkinje cell layer; ML, molecular layer. Scale bar: 100 µm. N=2.

4. Discussion

Recent studies have indicated the presence of $Ca_v1.3$ in the murine retina (see references in Table 1). My goal was to determine if HA-tagged $Ca_v1.3$ is detectable in retina cell membrane preparations. Furthermore, I aimed to localize HA-tagged and native $Ca_v1.3$ channels in retina cryo-sections. At last, I set out to assess if epitope-tagging and knock-out of $Ca_v1.3$ channels confers morphological changes within the retina. Parts of my work will be submitted to the Journal of Neuroscience in a joint publication.

4.1. Immunoblotting Analysis

Immunoblotting experiments revealed the presence of HA-tagged $Ca_v1.3$ in retina cell membrane preparations, as well as in positive control tissue, i.e. the brain. Analysis of transfer efficiency in Western Blotting experiments, however, revealed an inconsistency in the transfer of larger proteins as compared to smaller ones. Larger proteins were retained in the SDS polyacrylamide gel while smaller ones were transferred completely. This is of great importance because our HA-tagged $Ca_v1.3$ α1 subunit has an approximate size of 250 kDa, whereas our loading control protein, i.e. β-tubulin, has a size of 55 kDa. As a consequence, the subsequent densitometric evaluation of ECL bands is skewed towards a less robust intensity signal of HA bands (because less larger proteins were present on the membrane to produce an ECL-reactive signal as compared to smaller proteins). A solution to this problem could be an increase in transfer time (in conjunction with additional cooling to prevent system overheating).

Another interesting aspect that arose during my Western Blotting experiments was the observation of differing 'intertissue' loading control intensities. Loading control proteins, e.g. actin, tubulin, GAPDH, etc., are generally used to control for technical errors, e.g. unequal protein load or inconsistent protein transfer. The β-tubulin signals of brain membrane preparations are more prominent than those of the retina. This is intriguing because 30 µg of proteins were loaded in each well. However, recent observations (*60*), although made during quantitative Western Blotting experiments, highlighted that both β-actin and β-tubulin are differentially expressed across different tissues. I suspect that this could be the case between the brain and the retina. However, since ECL-based Western Blotting is a semi-quantitative method this difference in β-tubulin levels does not influence the statement that HA-tagged $Ca_v1.3$ is indeed present in the retina.

4.2. Immunohistochemical Analysis

Due to an inherently high variability of tissues there is no standardized procedure of immunohistochemistry. Defining the best experimental design turned out to be difficult for native and HA-tagged Ca$_v$1.3 retina and brain cryo-sections. During the course of my diploma thesis I tested a plethora of different IHC conditions (refer to tables 27 and 30).

We reasoned that native and HA epitopes might be masked due to protein crosslinks introduced upon paraformaldehyde fixation to maintain tissue morphology. Consequently, highly specific antibodies, recognizing small structural themes, might not be able to bind to the target sequence in the protein of interest. This phenomenon has been known for decades therefore several antigen retrieval methods have been developed. We decided to employ several buffers for heat induced antigen retrieval (refer to table 28) as described in (*61*) and elsewhere. However, even these rather stringent treatment protocols yet yielded no specific Ca$_v$1.3 or HA signals.

Another reason as to why we were not able to obtain specific signals might be the antibody itself. Our monoclonal HA antibody has been designed for Western and Dot Blots, ELISAs, immunoprecipitations and immunocytochemistry experiments. The absence of IHC from this list might already give an indication that our commercial source cannot guarantee the antibody to work on tissue sections. On the other hand, our Ca$_v$1.3 antibody directed against the N-terminus of native channels has been developed for paraffin embedded tissue IHC and Western Blots. In principle, this polyclonal antibody was designed to target the first 41 amino acids of native rat Ca$_v$1.3 channels which shows low sequence homology to Ca$_v$1.2 and Ca$_v$1.4 (*62*). Also, however, this antibody was not capable of producing specific staining in wild-type retina cryo-sections as compared to the knock-out. Interestingly, specific staining could be observed in the hippocampus while in cerebellum cryo-sections this antibody might recognize structures other than the N-terminus of Ca$_v$1.3.

Taken together, so far localization of HA-tagged Ca$_v$1.3 could not be established in retina and brain cryo-sections, possibly due to an issue with the antibody itself. Also, no specific staining of native channels could be obtained with a Ca$_v$1.3 antibody in the retina or cerebellum. However, we suggest that Ca$_v$1.3-specific staining was observable in the hippocampus of wild-type mice.

Assessment of retinal morphology based on standard markers worked in a satisfying manner once the right dilutions had been determined. Staining for PKC α, Calbindin, Calretinin, Parvalbumin and tyrosine hydroxylase revealed no apparent differences between the wild-type, Ca$_v$1.3-HA and Ca$_v$1.3 knock-out. PMCA1 staining was not changed in the inner retina, however, elucidated an apparent up-regulation of this molecule in the outer nuclear layer of Ca$_v$1.3 knock-out animals. Further experiments are on demand to reveal the mechanism behind this observation. However, these data point to a potential contribution of Cav1.3 to calcium extrusion mechanisms in photoreceptor terminals.

5. References

1. B. Alberts *et al.*, *Molecular Biology of the Cell* (Garland Science, Taylor & Francis Group, LLC, 5th Editio., 2007).

2. M. J. Berridge, M. D. Bootman, H. L. Roderick, Calcium signalling: dynamics, homeostasis and remodelling. *Nat. Rev. Mol. Cell Biol.* **4**, 517–29 (2003).

3. F. H. Yu, W. a Catterall, The VGL-chanome: a protein superfamily specialized for electrical signaling and ionic homeostasis. *Sci. STKE.* **2004**, re15 (2004).

4. W. A. Catterall, E. Perez-Reyes, T. P. Snutch, J. Striessnig, International Union of Pharmacology. XLVIII. Nomenclature and structure-function relationships of voltage-gated calcium channels. *Pharmacol. Rev.* **57**, 411–25 (2005).

5. W. a Catterall, Voltage-gated calcium channels. *Cold Spring Harb. Perspect. Biol.* **3**, a003947 (2011).

6. T. Kanamori *et al.*, Compartmentalized calcium transients trigger dendrite pruning in Drosophila sensory neurons. *Science.* **340**, 1475–8 (2013).

7. A. C. Dolphin, Calcium channel diversity: multiple roles of calcium channel subunits. *Curr. Opin. Neurobiol.* **19**, 237–44 (2009).

8. Z. Buraei, J. Yang, The ß subunit of voltage-gated Ca2+ channels. *Physiol. Rev.* **90**, 1461–506 (2010).

9. A. C. Dolphin, G protein modulation of voltage-gated calcium channels. *Pharmacol. Rev.* **55**, 607–27 (2003).

10. C. S. Bauer, A. Tran-Van-Minh, I. Kadurin, A. C. Dolphin, A new look at calcium channel α2δ subunits. *Curr. Opin. Neurobiol.* **20**, 563–71 (2010).

11. D. Lipscombe, S. E. Allen, C. P. Toro, Control of neuronal voltage-gated calcium ion channels from RNA to protein. *Trends Neurosci.* **36**, 598–609 (2013).

12. A. Singh *et al.*, Modulation of voltage- and Ca2+-dependent gating of CaV1.3 L-type calcium channels by alternative splicing of a C-terminal regulatory domain. *J. Biol. Chem.* **283**, 20733–44 (2008).

13. B. Z. Tan *et al.*, Functional characterization of alternative splicing in the C terminus of L-type CaV1.3 channels. *J. Biol. Chem.* **286**, 42725–35 (2011).

14. W. Xu, D. Lipscombe, Neuronal Ca(V)1.3alpha(1) L-type channels activate at relatively hyperpolarized membrane potentials and are incompletely inhibited by dihydropyridines. *J. Neurosci.* **21**, 5944–51 (2001).

15. G. Bock *et al.*, Functional properties of a newly identified C-terminal splice variant of Cav1.3 L-type Ca2+ channels. *J. Biol. Chem.* **286**, 42736–48 (2011).

16. J. Platzer *et al.*, Congenital deafness and sinoatrial node dysfunction in mice lacking class D L-type Ca2+ channels. *Cell.* **102**, 89–97 (2000).

17. P. Busquet *et al.*, CaV1.3 L-type Ca2+ channels modulate depression-like behaviour in mice independent of deaf phenotype. *Int. J. Neuropsychopharmacol.* **13**, 499–513 (2010).

18. S. M. Baig *et al.*, Loss of Ca(v)1.3 (CACNA1D) function in a human channelopathy with bradycardia and congenital deafness. *Nat. Neurosci.* **14**, 77–84 (2011).

19. E. a B. Azizan *et al.*, Somatic mutations in ATP1A1 and CACNA1D underlie a common subtype of adrenal hypertension. *Nat. Genet.* **45**, 1055–60 (2013).

20. D. Lipscombe, T. D. Helton, W. Xu, L-type calcium channels: the low down. *J. Neurophysiol.* **92**, 2633–41 (2004).

21. a Koschak *et al.*, alpha 1D (Cav1.3) subunits can form l-type Ca2+ channels activating at negative voltages. *J. Biol. Chem.* **276**, 22100–6 (2001).

22. J. E. Dowling, Retina : An Overview. *Encycl. Neurosci.* (2009), pp. 159–169.

23. H. Wässle, Parallel processing in the mammalian retina. *Nat. Rev. Neurosci.* **5**, 747–57 (2004).

24. O. Strauss, The retinal pigment epithelium in visual function. *Physiol. Rev.* **85**, 845–81 (2005).

25. R. Rosenthal *et al.*, Ca2+ channels in retinal pigment epithelial cells regulate vascular endothelial growth factor secretion rates in health and disease. *Mol. Vis.* **13**, 443–56 (2007).

26. R. H. Masland, The neuronal organization of the retina. *Neuron.* **76**, 266–80 (2012).

27. H. Wässle, C. Puller, F. Müller, S. Haverkamp, Cone contacts, mosaics, and territories of bipolar cells in the mouse retina. *J. Neurosci.* **29**, 106–17 (2009).

28. M. a MacNeil, R. H. Masland, Extreme diversity among amacrine cells: implications for function. *Neuron.* **20**, 971–82 (1998).

29. M. a MacNeil, J. K. Heussy, R. F. Dacheux, E. Raviola, R. H. Masland, The shapes and numbers of amacrine cells: matching of photofilled with Golgi-stained cells in the rabbit retina and comparison with other mammalian species. *J. Comp. Neurol.* **413**, 305–26 (1999).

30. W. N. Grimes, J. Zhang, C. W. Graydon, B. Kachar, J. S. Diamond, Retinal parallel processors: more than 100 independent microcircuits operate within a single interneuron. *Neuron.* **65**, 873–85 (2010).

31. M. García, E. Vecino, Role of Müller glia in neuroprotection and regeneration in the retina. *Histol. Histopathol.* **18**, 1205–18 (2003).

32. H. Kolb, Glial Cells of the Retina (2001), (available at http://www.ncbi.nlm.nih.gov/books/NBK11516/).

33. C. J. Habermann, B. J. O'Brien, H. Wässle, D. a Protti, AII amacrine cells express L-type calcium channels at their output synapses. *J. Neurosci.* **23**, 6904–13 (2003).

34. C. W. Morgans *et al.*, Photoreceptor calcium channels: insight from night blindness. *Vis. Neurosci.* **22**, 561–8 (2005).

35. H. Xiao, X. Chen, E. C. Steele, Abundant L-type calcium channel Ca(v)1.3 (alpha1D) subunit mRNA is detected in rod photoreceptors of the mouse retina via in situ hybridization. *Mol. Vis.* **13**, 764–71 (2007).

36. D. Specht *et al.*, Effects of presynaptic mutations on a postsynaptic Cacna1s calcium channel colocalized with mGluR6 at mouse photoreceptor ribbon synapses. *Invest. Ophthalmol. Vis. Sci.* **50**, 505–15 (2009).

37. F. F. J. Kersten *et al.*, Association of whirlin with Cav1.3 (alpha1D) channels in photoreceptors, defining a novel member of the usher protein network. *Invest. Ophthalmol. Vis. Sci.* **51**, 2338–46 (2010).

38. J. Zou, A. Lee, J. Yang, The expression of whirlin and Cav1.3α$_1$ is mutually independent in photoreceptors. *Vision Res.* **75**, 53–9 (2012).

39. S. Siegert *et al.*, Transcriptional code and disease map for adult retinal cell types. *Nat. Neurosci.* **15**, 487–95, S1–2 (2012).

40. D. G. Puro, J. J. Hwang, O. J. Kwon, H. Chin, Characterization of an L-type calcium channel expressed by human retinal Müller (glial) cells. *Brain Res. Mol. Brain Res.* **37**, 41–8 (1996).

41. B. B. Lewis *et al.*, Cloning and characterization of voltage-gated calcium channel alpha1 subunits in Xenopus laevis during development. *Dev. Dyn.* **238**, 2891–902 (2009).

42. C. W. Morgans, Calcium channel heterogeneity among cone photoreceptors in the tree shrew retina. *Eur. J. Neurosci.* **11**, 2989–2993 (1999).

43. N. C. Welch *et al.*, High-voltage-activated calcium channels in Muller cells acutely isolated from tiger salamander retina. *Glia.* **49**, 259–74 (2005).

44. M. Cristofanilli, F. Mizuno, A. Akopian, Disruption of actin cytoskeleton causes internalization of Ca(v)1.3 (alpha 1D) L-type calcium channels in salamander retinal neurons. *Mol. Vis.* **13**, 1496–507 (2007).

45. F. Mizuno, P. Barabas, D. Krizaj, A. Akopian, Glutamate-induced internalization of Ca(v)1.3 L-type Ca(2+) channels protects retinal neurons against excitotoxicity. *J. Physiol.* **588**, 953–66 (2010).

46. H.-P. Xu, J.-W. Zhao, X.-L. Yang, Expression of voltage-dependent calcium channel subunits in the rat retina. *Neurosci. Lett.* **329**, 297–300 (2002).

47. A. Scharinger, thesis, University of Innsbruck (2013).

48. N. T. Bech-Hansen *et al.*, Loss-of-function mutations in a calcium-channel alpha1-subunit gene in Xp11.23 cause incomplete X-linked congenital stationary night blindness. *Nat. Genet.* **19**, 264–7 (1998).

49. T. M. Strom *et al.*, An L-type calcium-channel gene mutated in incomplete X-linked congenital stationary night blindness. *Nat. Genet.* **19**, 260–3 (1998).

50. C. W. Morgans, Localization of the alpha(1F) calcium channel subunit in the rat retina. *Invest. Ophthalmol. Vis. Sci.* **42**, 2414–8 (2001).

51. X. Liu *et al.*, Dysregulation of Ca(v)1.4 channels disrupts the maturation of photoreceptor synaptic ribbons in congenital stationary night blindness type 2. *Channels (Austin).* **7**, 514–23 (2013).

52. O. H. LOWRY, N. J. ROSEBROUGH, A. L. FARR, R. J. RANDALL, Protein measurement with the Folin phenol reagent. *J. Biol. Chem.* **193**, 265–75 (1951).

53. S. Haverkamp, H. Wässle, Immunocytochemical Analysis of the Mouse Retina. *J. Comp. Neurol.* **424**, 1–23 (2000).

54. D. Krizaj, S. J. Demarco, J. Johnson, E. E. Strehler, D. R. Copenhagen, Cell-specific expression of plasma membrane calcium ATPase isoforms in retinal neurons. *J. Comp. Neurol.* **451**, 1–21 (2002).

55. C. W. Morgans, O. El Far, A. Berntson, H. Wässle, W. R. Taylor, Calcium extrusion from mammalian photoreceptor terminals. *J. Neurosci.* **18**, 2467–74 (1998).

56. S. Haverkamp, D. Inta, H. Monyer, H. Wässle, Expression analysis of green fluorescent protein in retinal neurons of four transgenic mouse lines. *Neuroscience.* **160**, 126–39 (2009).

57. N. Billinton, a W. Knight, Seeing the wood through the trees: a review of techniques for distinguishing green fluorescent protein from endogenous autofluorescence. *Anal. Biochem.* **291**, 175–97 (2001).

58. M. J. Kim *et al.*, Immunohistochemical study of the distribution of neuronal voltage-gated calcium channels in the nNOS knock-out mouse cerebellum. *Neurosci. Lett.* **369**, 39–43 (2004).

59. F. L. Núñez-Santana *et al.*, Surface L-type Ca2+ channel expression levels are increased in aged hippocampus. *Aging Cell.* **13**, 111–20 (2014).

60. S. L. Eaton *et al.*, Total protein analysis as a reliable loading control for quantitative fluorescent Western blotting. *PLoS One.* **8**, e72457 (2013).

61. I. B. Buchwalow, W. Böcker, *Immunohistochemistry: Basics and Methods* (Springer Berlin Heidelberg, Berlin, Heidelberg, 2010; http://link.springer.com/10.1007/978-3-642-04609-4).

62. I. Calin-Jageman, K. Yu, R. a Hall, L. Mei, A. Lee, Erbin enhances voltage-dependent facilitation of Ca(v)1.3 Ca2+ channels through relief of an autoinhibitory domain in the Ca(v)1.3 alpha1 subunit. *J. Neurosci.* **27**, 1374–85 (2007).

6. Appendix

6.1. Abstract

Ca$_v$1.3 belongs to the family of voltage-gated calcium channels (VGCCs) which are important mediators in the processes of hearing, cardiac pacemaking and hormone secretion by various endocrine cells. Recent studies have furthermore indicated the presence of Ca$_v$1.3 in the mammalian retina. To date, however, exact localization to specific retinal layers has turned out to be inconclusive. Consequently, the role of Ca$_v$1.3 as a potential contributor to vision is vividly debated.

In this study I used two genetically modified mice to pinpoint Ca$_v$1.3 retinal localization. On the one hand, I employed an epitope-tagged mouse model that contains a HA-tag (hemagglutinin, derived from influenza virus) in the C-terminus of Ca$_v$1.3. I was able to show that HA-tagged Ca$_v$1.3 is indeed present in the retina. Following on this I set out to determine its retinal localization by means of immunohistochemistry. Establishing Ca$_v$1.3-HA-specific staining, however, turned out to be problematic. I hypothesize that this is based on the limited suitability of the antibody as it is not able to detect HA-specific signals in control tissues.

The second mouse model is characterized by a knock-out, i.e. the absence, of Ca$_v$1.3. Immunohistochemical analyses of retinae were also afflicted by poor antibody recognition. In fact, the antibody directed against the N-terminus of native Ca$_v$1.3 was not capable of detecting its supposed target. However, this antibody yielded interesting results in my control tissue, i.e. the brain. Ca$_v$1.3-specific signals are detectable in the hippocampus of wild-type mice while being absent in knock-out brains. In the cerebellum, Ca$_v$1.3-specific signals are also present in the knock-out mouse, an observation that puts this antibody under intense scrutiny.

At last, I wanted to assess if these two mouse models show any abnormalities as compared to the wild-type. For this, I looked at several standard markers in retinal immunohistochemistry. All analyzed proteins but one, i.e. PMCA1 in the Cav1.3 knock-out, are normal as compared to the wild-type. PMCA1, which is a calcium pump protecting cells from elevated intracellular calcium ion concentrations, retains inner retinal localization but shows an apparent up-regulation in the outer nuclear layer, i.e. the layer containing photoreceptor cell bodies. Further studies and an established collaboration will hopefully shed light onto this interesting observation and might hint at the physiological function of Cav1.3 in the mammalian retina.

6.2. Zusammenfassung

Ca$_v$1.3 ist ein Mitglied der spannungsabhängigen Kalziumkanäle (VGCCs) und fungiert als Mediator in wichtigen zellulären Prozessen wie Hören oder der Freisetzung von Hormonen aus endokrinen Zellen. Weiters wird dieser Kalziumkanal im Atrioventrikularknoten des Herzens exprimiert wo er für die Erregungsleitung im Ruhezustand verantwortlich ist. Neueste Studien deuten auf das Vorhandensein von Ca$_v$1.3 in der Wirbeltiernetzhaut, der Retina, hin. Allerdings ist es Wissenschaftlern noch nicht gelungen die genaue Position des Kanals innerhalb der vielen, äußerst spezifischen Schichten der Retina zu bestimmen. Aufgrund dessen wird die Rolle von Ca$_v$1.3 im Prozess der Sinneswahrnehmung durch das Auge lebhaft diskutiert.

In dieser Arbeit habe ich mich mit zwei genetisch veränderten Mausmodellen befasst, um Ca$_v$1.3 in der Retina zu lokalisieren. Die erste Maus hat einen so genannten HA-tag, benannt nach dem Hämagglutinin des Influenzavirus, im C-terminus des Ca$_v$1.3 Proteins inseriert. Durch diesen leicht detektierbaren Marker konnte ich zeigen, dass Ca$_v$1.3 tatsächlich in der Retina exprimiert wird. Basierend auf dieser Beobachtung wollte ich weiters die genaue Lokalisation des Proteins in den einzelnen Schichten der Retina feststellen. Mein experimenteller Zugang hierfür war die Immunhistochemie – das Sichtbarmachen von Proteinen durch fluoreszenzmarkierte Antikörper. Dieser Ansatz stellte sich allerdings als problematisch heraus, da der verwendete Antikörper im Kontrollgewebe, dem Hirn, kein Signal gab. Daraus schließe ich, dass dieser Antikörper nur bedingt geeignet ist.

Das zweite Mausmodell war ein so genannter knock-out. In diesem Fall fehlt der funktionelle Ca$_v$1.3 Kalziumkanal. Auch in diesem experimentellen Ansatz war der verwendete Antikörper nicht geeignet für Immunhistochemie. Dieser sollte an den N-terminus von Ca$_v$1.3 Proteinen in der wildtypischen Maus binden. Im Kontrollgewebe hingegen konnte ich interessante Beobachtungen anstellen. So scheint es, dass der Antikörper spezifisch Ca$_v$1.3 im wildtypischen Hippocampus erkennt und im knock-out nicht. Im Kleinhirn wiederum scheint der Antikörper auch spezifisch Zellen im knock-out zu erkennen was natürlich einige Fragen aufwirft.

Abschließend widmete ich mich der generellen Morphologie der Retina und wollte untersuchen ob die Mausmodelle Veränderungen hinsichtlich bekannter Markerproteine aufweisen. Lediglich PMCA1, eine Kalziumpumpe die Zellen vor einer zu hohen intrazellulären Kalziumionenkonzentration schützt, weist eine erhöhte Expression in der äußeren Kernschicht der Cav1.3 knock-out Retina auf. Weitere Studien und eine Kollaboration werden hoffentlich den zugrungeliegenden Mechanismus hinsichtlich der PMCA1 Beobachtung entschlüsseln und somit auch die Rolle von Cav1.3 in der Retina eruieren.

6.3. Curriculum vitae

Personal Information:

Place of birth: Mödling, Lower Austria

Date of birth: October 29, 1989

Nationality: Austrian

Education:

October 2012 – present
University of Vienna, Master of Science (MSc) in Molecular Biology

Major: Neurosciences

October 2009 – July 2012
University of Vienna, Bachelor of Science (BSc) in Biology

Major: Molecular Biology

November 2008 – May 2009
Military service in Zwölfaxing (Lower Austria) and Baden (Lower Austria)

2000 – 2008
BG/BRG Keimgasse in Mödling with emphasis on natural sciences

1996 – 2000
Elementary school in Mödling, Lower Austria

Practical Experience:

July 2013 – present:

Medical University Vienna (Center for Physiology and Pharmacology/Dept. for Neurophysiology and Neuropharmacology), **Master thesis**

Thesis: Localization of $Ca_v1.3$ L-type calcium channels in the mouse retina

Supervisor: Univ. Prof. Mag. Dr. Alexandra Koschak

October 2012 – June 2013:

Medical University Vienna (Center for Physiology and Pharmacology/Dept. for Neurophysiology and Neuropharmacology), **Laboratory Assistant**

Lab: Univ. Prof. Mag. Dr. Alexandra Koschak

May 2012 – July 2012:

Medical University Vienna (Center for Physiology and Pharmacology/Dept. for Neurophysiology and Neuropharmacology), **Bachelor thesis**

Topic: Establishment of various SOPs for expression, isolation and detection of Cav1.4 L-type voltage-gated calcium channels

Supervisor: Univ. Prof. Mag. Dr. Alexandra Koschak

Publications:

V. Burtscher et al., Spectrum of Cav1.4 dysfunction in congenital stationary night blindness type 2. Biochim. Biophys. Acta. 1838, 2053–2065 (2014).

6.4. List of figures

6.5. List of tables